# How melt segregation impacts on granite chemistry: migmatites from the Sierra de Quilmes, NW Argentina

L. C. Wolfram[1]*, R. F. Weinberg[1], P. Hasalová[2], R. Becchio[3]

[1]School of Earth, Atmosphere and Environment, Monash University, Clayton, Victoria, Australia 3800

[2]Centre for Lithospheric Research, Czech Geological Survey, Klarov 3, 118 21 Prague 1, Czech Republic

[3]Instituto Geonorte, National University of Salta, INENCO-CONICET, Av. Bolivia 5150, 4400 Salta, Argentina

* Corresponding author. Email: lauren.wolfram@gmail.com

Running title: How melt segregation impacts on granite chemistry

**ABSTRACT**

Compositional variability of crustal-derived granites has been attributed to a multitude of processes. Though there has been much discussion on the entrainment of residuum and its effect on granite magma chemistry, the exact nature of what is entrained and when entrainment is efficient remains unclear. We describe the relationship between granulite facies migmatites and granites in the Sierra de Quilmes, NW Argentina, focussing on how the style of melt segregation impacts its ability to disaggregate the source and carry residual minerals, and therefore control granite chemistry. The north-south trending mountains that define the region known as the Sierras Pampeanas are characterised by variably metamorphosed turbidites of the Neoproterozoic–Cambrian Puncoviscana Formation. Early Ordovician subduction on the western Gondwana margin produced widespread high-T, low-P metamorphism of the turbidites during the Famatinian orogeny (~500–440 Ma), resulting in extensive anatexis and granite plutonism. The Tolombón complex of the northern Sierra de Quilmes is a tilted metamorphic sequence in the northern Sierras Pampeanas, providing near-complete exposure from granulite facies magma source rocks in the southwest to granite emplacement levels in amphibolite and greenschist facies rocks in the northeast. Anatexis is associated with fluid-absent incongruent breakdown of biotite in granulite facies rocks, evidenced by the presence of peritectic Grt±Crd±Opx. The western Tolombón complex is separated from the Ovejeria complex by a shear zone. The Ovejeria complex is distinguished by a generally higher melt fraction, and is dominated by gradational contacts from metatexites to diatexites and granites. In contrast, in the Tolombón complex, with few examples of diatexites, magmas are more commonly extracted from metatexites, and migrate to feed stocks and plutons at higher crustal levels. Granites derived from diatexites tend to remain close to the source and retain strong compositional similarities to the Puncoviscana Formation protolith, indicating significant

mobilisation of residuum, and defining the Ovejeria style of granite formation. Granites derived dominantly from melt extraction from metatexites tend to be leucogranites with compositions approaching those of experimental melts, defining the Tolombón style of granite formation. Magma derived through either mechanism undergoes further differentiation, giving rise to the compositionally diverse suite of rocks common to most anatectic terranes. Magmas derived through the Tolombón style of melt extraction are leucocratic, and impoverished in LREE, Th, and Zr compared to both the sedimentary source rocks and residuum-rich magmas derived through the Ovejeria style of granite formation. The low solubility of zircon and monazite in relatively dry, peraluminous leucogranite melts guarantees that Zr, Th, and LREE behave as compatible elements during dehydration melting of metasedimentary packages. Therefore, neither style of granite formation contributed to the transfer of many of the typical trace elements enriched in the upper crust. Instead, biotite dehydration melting in the Sierra de Quilmes had the opposite effect of typical crustal differentiation, concentrating these trace elements in the residual source, possibly reflecting the lack of a pressure gradient driving extraction of residuum-rich magmas.

Keywords: zircon, monazite dissolution; crustal differentiation; partial melting; residuum entrainment

## INTRODUCTION

Partial melting plays an important role in crustal differentiation (e.g. Sawyer, 1998; Korhonen *et al.*, 2010). Dehydration melting experiments on metapelites and metagreywackes show that 40–60 vol.% anatectic melt can be produced at temperatures up

to 900 ˚C (Patiño Douce & Johnston, 1991; Vielzeuf & Montel, 1994; Gardien *et al.*, 1995). Granitic magma formed through partial melting is subsequently transported to higher crustal levels, enriching the upper crust in incompatible elements, including heat-producing elements (McLennan *et al.*, 2006), with important implications for the thermal structure and stability of the continental crust (Sandiford & McLaren, 2006). It is therefore important to understand the mechanisms responsible for elemental distribution within anatectic suites and how they are transferred to granites and through the crust.

Granites derived through partial melting of the continental crust have a wide range of compositions attributed to multiple processes including magma mixing and mingling (Vernon *et al.*, 1988), assimilation of country rock (DePaolo, 1981), the rate of melt production versus extraction (Watt *et al.*, 1996), entrainment of residuum (Chappell *et al.*, 1987; Sawyer, 1998; Dorais & Spencer, 2014), fractional crystallisation (e.g. Tindle & Pearce, 1981), dynamic melting (e.g. Bhadra *et al*., 2007) and initial protolith composition and fertility (Thompson, 1996). More than one of these processes will commonly influence the composition of the magma at various stages of its evolution.

The restite-unmixing model of White & Chappell (1977) and Chappell *et al.* (1987) attributes the compositional variation of granites to complete mobilisation of the source rock, followed by gradual filtering of the restite. Restite includes both unmelted residual and peritectic minerals. Peritectic assemblage entrainment (PAE) is a refined version of the restite-unmixing model, and credits the elevated ferromagnesian contents of granites to selective entrainment of small peritectic phases (Stevens *et al.*, 2007; Taylor & Stevens, 2010). This model does not consider the actual extraction processes that take place in the source of granitic melts; it was critically reviewed in Regmi *et al.* (2016).

The complete breakdown of the rock framework, resulting from sufficiently high melt fractions, forms diatexite magmas (Brown, 1973) that can have near-identical

compositions to their source (Chappell *et al.*, 1987). Required melt fractions of 10–35 vol.% were proposed by Arzi (1978: 'rheological critical melt percentage') and van der Molen & Paterson (1979: 'critical melt fraction'). Miller *et al.* (1988, and references therein) demonstrated that this critical value also depends on textural characteristics such as grain size distribution, grain shapes, and average wetting angle, which control the contiguity of the system. Considering an average wetting angle of 50° (typical of crustal melting; Jurewicz & Watson, 1984), Miller *et al*., (1988) estimated a critical melt fraction of at least 50 vol.% in a static system.

In contrast, segregation of anatectic melt from the solid fraction will produce a liquid depleted in $FeO_T$ and MgO and enriched in $SiO_2$ and $K_2O$ (e.g. Solar & Brown, 2001), and leave behind a complementary residuum enriched in $FeO_T$ and MgO and depleted in $SiO_2$ and $K_2O$ (Guernina & Sawyer, 2003; Brown, 2013). In migmatites, melt segregation and extraction are expressed as leucosomes and melanosomes in metatexites (Sawyer, 1994; Brown, *et al*., 1995). Melt can also be separated from residue in diatexites, less efficiently, through magma flow (Sawyer, 1996). Though there has been much discussion on the entrainment of residuum and its effect on granite magma chemistry, the exact nature of what is entrained and when entrainment is efficient remains unclear. This is depeneant on the nature of the melt extraction networks, which in turn depend on the rate of melt production versus extraction (Watt *et al.*, 1996), a function of complex feedback relations between melting reactions, melt production rates, and volume change, on the one hand, and regional drivers of magma migration (differential stresses and pressure gradients), and rock strength and anisotropy (Sawyer, 1991; Marchildon & Brown, 2003) on the other.

The Sierra de Quilmes in NW Argentina contains a near-complete high-T, low-P metamorphic sequence from granulite facies anatectic source rocks to emplacement of

granite bodies in amphibolite and greenschist facies rocks at higher crustal levels (Finch *et al.*, 2017; Büttner *et al.*, 2005). This study combines field observations, petrography, and whole-rock major and trace element geochemistry to investigate how different styles of melt segregation impact the evolution of magmas to produce compositionally diverse granites. In addition, we address the behaviour of accessory minerals during melting, and explore the implications for redistribution of accessory-hosted trace elements in the context of crustal differentiation. We begin with a broad description of the Sierra de Quilmes in a regional context, followed by a detailed description of the rock types comprising the granulite facies terrane. After presenting whole-rock geochemistry, we discuss the results in terms of different styles of granite-forming processes and their implications for the entrainment of residuum.

## REGIONAL GEOLOGY

The Sierras Pampeanas (Fig. 1) comprise twelve north-south trending mountains in northwest and central Argentina that were uplifted during the Andean orogeny (Jordan & Allmendinger, 1986). They are divided into Western and Eastern Sierras Pampeanas based on differences in sedimentary provenance and tectono-metamorphic evolution (Fig. 1; Rapela *et al.*, 2016). The Western Sierras Pampeanas are dominated by metabasic, ultrabasic and calc-silicate rocks of Mesoproterozoic to Early Paleozoic age, whilst the Eastern Sierras Pampeanas consist chiefly of Paleozoic metasedimentary rocks and widespread granite plutons (Rapela *et al.*, 2016). Metamorphic grade generally increases from north to south within the Sierras Pampeanas (Piñan-Llamas & Simpson, 2006).

The protolith to the Eastern Sierras Pampeanas is the Puncoviscana Formation turbidite sequence, chiefly an interbedded psammite-pelite succession with local conglomerate, carbonate, and volcanogenic material (Toselli *et al.*, 1978; Ježek *et al.*, 1985; Aceñolaza *et al.*, 1988). The >2000 m thick sedimentary basin extends from southern Bolivia to central Argentina, covering a total area of 1200 km N–S and 300 km E–W (Ježek *et al.*, 1985). Deposition marks the Neoproterozoic break-up of Rodinia (Rapela *et al.*, 1998a) and subsequent opening of the Puncoviscan and Southern Iapetus oceans off the western Gondwana margin (Rapela *et al.*, 1998b; Cawood, 2005). Geochronology and provenance studies indicate that the Brazilian Shield was the main source of Puncoviscana Formation sediments (Aceñolaza *et al.*, 1988; Adams *et al.*, 2011), deposited along the passive proto-Andean margin between the Late Neoproterozoic and Early Cambrian until ~520 Ma (Adams *et al.*, 2011). There is currently no minimum depositional age due to the lack of exposure of the base of the sequence (Ježek *et al.*, 1985).

Subduction along the western Gondwana margin began in the Early Cambrian (Rapela *et al.*, 1998a; Cawood, 2005), leading to closure of the Puncoviscan Ocean and initiating a protracted phase of Paleozoic orogenesis (Aceñolaza *et al.*, 1988; Rapela *et al.*, 1998a). The first event, known as the Pampean orogeny, is marked by the intrusion of subduction-related calc-alkaline granitoids at ~535 Ma (Rapela *et al.*, 1998a, b). Collision of the Pampean terrane with the western Gondwana margin led to granulite facies metamorphism of the Puncoviscana Formation (Piñan-Llamas & Simpson, 2006), and associated anatexis produced highly peraluminous granites across the Eastern Sierras Pampeanas (~520 Ma; Rapela *et al.*, 1998a). Intrusion of I-type granitoids in Sierra Norte de Córdoba provides a youngest age of 515 ± 4 Ma for the Pampean orogeny, which was followed by a break in magmatism, and potentially subduction, lasting ~20 Myr. (Sims *et al.*, 1998). Additional sedimentation along the western Gondwana margin, sourced

predominantly from Pampean rocks, occurred during this time (Pankhurst *et al.*, 1998; Sims *et al.*, 1998).

The second event, known as the Famatinian orogeny, was initiated by renewed eastward subduction during the Late Cambrian–Early Ordovician, marked by the trenchward (westward) formation of a new magmatic arc at ~495 Ma (Rapela *et al.*, 1998a, b; Pankhurst *et al.*, 1998), and widespread amphibolite to granulite facies metamorphism and anatexis between ~500–440 Ma (Pankhurst *et al.*, 2000; Finch *et al.*, 2017). The Famatinian orogeny extended N–S from 22° to 33° S (present-day coordinates), along the entire length of the Sierras Pampeanas (Rapela *et al.*, 1998a; Hongn *et al.*, 2010). High-T, low-P metamorphism is ubiquitous along the ~1000 km-long back-arc (Fig. 1; e.g. Pankhurst *et al.*, 2000; Büttner *et al.*, 2005; Sola *et al.*, 2013). Evidence from the northern Sierras Pampeanas and Puna indicate an extensional back-arc setting during the early Famatinian (e.g. Ordovician marine basin deposits: Bahlburg, 1998; bi-modal rift-related magmatism: Coira *et al*., 2009), which underwent basin inversion and shortening towards the end of the orogeny (e.g. Rapela *et al*., 1998b).

Magmatism associated with the Famatinian orogeny falls into three categories: (i) I-type, (ii) S-type, and (iii) tonalite-trondhjemite-granodiorite (TTG) type (Toselli *et al.*, 1978; Rapela *et al.*, 1990). I-type plutons range in composition from gabbro to tonalite (Pankhurst *et al.*, 2000), and locally grade into peraluminous S-type granites further east (Steenken *et al.*, 2011) where anatexis is related to the high-T, low-P metamorphism in the back-arc region (e.g. Pankhurst *et al.*, 2000; Büttner *et al.*, 2005; Finch *et al.*, 2017). Collision of the Precordillera terrane with the western Gondwana margin culminated in shortening and the cessation of arc magmatism (Rapela *et al.*, 1998a), reflecting the end of the Famatinian orogeny and closure of the back-arc basin (Thomas & Astini, 2003 and references therein; Varela *et al.*, 2011).

**Sierra de Quilmes**

The Sierra de Quilmes is a ~140 km long ridge in the northern Sierras Pampeanas located west of the town of Cafayate (Fig. 1; Rossi de Toselli *et al.*, 1976), exposing Famatinian metamorphism, anatexis, and ductile shearing (Büttner *et al.*, 2005; Finch *et al.*, 2015). It has been previously divided into two complexes of different metamorphic facies, separated by the west-thrusting El Pichao shear zone (Fig. 2; Finch *et al.*, 2015): the granulite facies Tolombón complex to the north, thrust obliquely over the amphibolite facies Agua del Sapo complex in the south (Toselli *et al.*, 1978; Finch *et al.*, 2015). In this study we focus on the higher-grade Tolombón complex.

The Tolombón complex comprises rocks of the Puncoviscana Formation in a tilted crustal section ranging from greenschist facies rocks in the east to granulite facies Grt-Crd-Opx migmatites in the west, with no evidence for influx of juvenile magmas (Büttner *et al.*, 2005; Finch *et al.*, 2017). Peak metamorphism at ~800–850 °C and ~6 kbar (Büttner *et al.*, 2005) occurred between ~500 and 450 Ma (TIMS U-Pb monazite and titanite ages: Büttner *et al.*, 2005; SHRIMP U-Pb monazite ages: Finch *et al.*, 2017). Here we separate the western part of the Tolombón into the Ovejeria complex, separated by an ill-defined NNW–SSE-trending mylonitic zone (Fig. 2). We first summarise the Tolombón complex in the east according to previously published studies, and then describe migmatites and granites from both complexes in detail.

Finch *et al*. (2017) further detailed the rock divisions of Büttner *et al*. (2005) and divided the Tolombón complex into six zones trending ~NNW–SSE with a general increase in metamorphic grade to the west, partly repeated by the Tolombón thrust (see Fig. 2; mineral abbreviations after Whitney & Evans, 2010). The Chl zone (not shown) comprises greenschist facies metasedimentary rocks that preserve primary sedimentary structures (see

Fig. 2 in Büttner *et al*., 2005). The appearance of metamorphic cordierite to the west designates the Crd-subsolidus zone, which is followed by the Sil+Crd-metatexite zone where metatexites containing peritectic sillimanite indicate the onset of muscovite dehydration melting. Garnet- and cordierite-bearing leucosomes mark the onset of the Grt-metatexite zone, and indicate a change to biotite dehydration melting. Melt fraction increases towards the west in this zone, culminating with the loss of internal coherence, forming diatexites (e.g. Brown, 1973). The westernmost metamorphic zone described by Büttner *et al.* (2005) and Finch *et al*. (2017) is the Opx-metatexite zone, characterised by leucosomes containing peritectic garnet, cordierite, and orthopyroxene in variable combinations and modal proportions. Orthopyroxene occurs primarily in psammitic layers of metatexites, and cordierite in pelitic layers, with garnet appearing throughout. Melt fraction increases locally to form diatexites as for the Grt-metatexite zone. The composite ~2.6 km wide Cafayate pluton (true width based on ~50° regional dip; e.g. Büttner *et al*., 2005) intrudes Sil-Crd metatexites in the Tolombón complex (Fig. 2) and grades in composition from tonalite to granite to the east (Rapela & Shaw, 1979; Finch *et al*., 2017).

## THE TOLOMBÓN AND OVEJERIA COMPLEXES

Migmatites of the Tolombón and Ovejeria complexes are essentially similar in composition and metamorphic grade. However, they differ significantly in their relative volumes of retained melt fraction and associated granites: the Ovejeria complex is dominated by diatexite magmas transitional to residuum-rich granites, in contrast with the Tolombón complex, dominated by metatexites. For migmatites in both complexes, peritectic garnet, cordierite, and orthopyroxene suggest partial melting via reactions such as (1) Bt + Sil +

Qtz + Fsp = Kfs + Grt ± Crd + melt, and (2) Bt + Qtz ± Fsp = Opx ± Fsp ± Grt ± Crd + melt (Clemens & Wall, 1981; Le Breton & Thompson, 1988). In this section, we describe the main rock types from both complexes together, and later explore the differences between the granite-forming styles of the two. Terminology for migmatites follows that of Sawyer (2008).

**Metatexites**

Metatexites have an overall grey appearance, with dark, biotite-rich melanosomes bordering biotite-poor (<3 vol.%) granitic leucosomes. They may preserve pre-partial melting structures (e.g. sedimentary layering) due to low proportions of retained melt fraction (Sawyer, 2008). Three different types are recognised: patch-nebulitic metatexites, net-structured metatexites, and stromatic metatexites.

The neosome (melted portion) of some metatexites has discrete patches of leucosome (patch metatexites), which can coalesce to form a nebulite as the volume fraction of leucosomes increases, interpreted to represent an increase in melt fraction (e.g. Sawyer, 2008). We refer to these collectively as patch-nebulitic metatexites (Fig. 3a, left-hand side). Due to a lack of oriented grains or disruption of leucosomes, these sites are interpreted to reflect relatively low levels of syn-anatectic strain (Sawyer, 2008). Patch-nebulitic metatexites most commonly form in metapsammitic layers, and consist of a fine-grained (~1 mm) paleosome, and a neosome of medium-grained (~5 mm) leucosomes surrounded by thin melanosomes <2 mm wide. Margins between paleosome and neosome vary from sharp to diffuse. Thin leucosomes connect with leucogranite bodies up to one metre wide (Fig. 3a, right-hand side), which contain melanocratic schlieren, inclusion-rich garnet porphyroblasts, and small (<10 mm), inclusion-free garnets.

Net-structured metatexites (Fig. 3b, c) are the least common, and are derived from metapsammitic or metapelitic protoliths predominantly in the Grt-metatexite zones. Leucosomes are generally more clearly segregated than in the patch-nebulitic metatexites, and melanocratic selvedges along the margins are up to 5 mm wide (e.g. leucosome in top half of Fig. 3c). Leucosomes vary between ~5–20 mm thick, the smaller ones feeding larger pools of granitic melt interpreted to represent dilatant sites (arrows in Fig. 3b), some of which may represent collapse structures due to melt extraction (Fig. 3c; e.g. Marchildon & Brown, 2003; Bons *et al*., 2008). The patterns developed by these are different whether viewed in planes perpendicular or parallel to the main stretching lineation. Extensional shear planes (Fig. 3b) and sigma clasts suggest higher syn-anatectic strain than in the patch-nebulitic metatexites (Sawyer, 2008).

Stromatic metatexites (e.g. Fig. 3d, e) are the most widespread, occurring in all metatexite zones. Leucosomes are medium-grained (~5 mm), and are more abundant in metapelitic than metapsammitic layers. They vary from ~1 mm to 30 mm wide, the latter commonly feeding into large pools of homogeneous leucogranitic magma (e.g. Fig. 3d) as for the patch-nebulitic metatexites. Melanosomes and paleosomes are comparably fine-grained (<2 mm), with biotite typically comprising >30 vol.%. The ratio of paleosome + melanosome to leucosome is variable between outcrops, with some stromatic metatexites containing barely any leucosome (<10 vol.%) and a high proportion of peritectic minerals, including large garnets, and a greater paleosome + melanosome content (Fig. 3e). We interpret these as residual metatexites reflecting significant melt loss.

Variable combinations and proportions of peritectic garnet, cordierite, and orthopyroxene are observed in the metatexites, depending on the metamorphic zone and specific rock composition. Garnet forms euhedral to subhedral porphyroblasts, which are typically poikiloblastic with coarse-grained quartz and rounded biotite inclusions indicating

a peritectic origin (Fig. 3f). They range in size from ~15–60 mm, with the largest in thick, oblique leucosomes in the net-structured metatexites (Fig. 3b). Though less common than garnet, orthopyroxene (5–10 mm) is present in the patch-nebulitic and stromatic metatexites in psammites in the Opx-metatexite zone (e.g. Fig. 3a). Grains vary from poikiloblastic, to euhedral–subhedral crystals with minor inclusions of quartz, zircon, and monazite. Both garnet and orthopyroxene are typically located within leucosomes that contain minor biotite (<3 vol.%). Leucocratic zones directly surrounding garnet and orthopyroxene are typically biotite free, and crystals are only occasionally overgrown by narrow Qtz+Bt symplectites interpreted to represent partial retrogression, indicating that the majority of melt was extracted (White & Powell, 2002). Cordierite forms roughly equant grains ~0.5–5 mm long in net-structured and stromatic metatexites, where it occurs in both leucosomes and melanosomes. Crystals contain a high proportion of inclusions of rounded quartz and feldspar (10–200 μm), elongate to tabular biotite (10–500 μm), as well as small accessory zircon, monazite, and apatite (~10–100 μm). Biotite and fine-grained Sil+Ms occur along cordierite rims, with more pervasive alteration affecting grains hosted within leucosomes. The majority of accessory minerals (zircon, monazite, apatite, and minor xenotime) are included within quartz, feldspar, and biotite, or occur along grain margins.

**Diatexites**

Diatexites have a heterogeneous appearance due to irregular dispersal of melanocratic schlieren and schollen (e.g. Fig. 4a). They contain varying quantities of peritectic minerals, display igneous textures, and have granitic bulk compositions gradually transitioning from residual, melanocratic diatexites (Fig. 4b) to leucocratic diatexites (Fig. 4a) and schlieric granites (Fig. 4c). Schollen, schlieren, and the peritectic minerals (Grt±Crd±Opx) plus biotite are henceforth collectively referred to as the residuum.

*Residual diatexites*

Residual diatexites have a granular appearance (Fig. 4b), and are dark grey, resulting from enrichment in ferromagnesian minerals (reaching >80 vol.%, Finch *et al*., 2017). The strongly residual versions are relatively uncommon, forming irregular pockets up to one metre wide within the Grt- and Opx-metatexite zones (Finch *et al*., 2017), and grade to leucocratic end-members (Fig. 4d, right-hand side). In contrast to the residual metatexites in the Tolombón complex, these diatexites are more common in the Ovejeria complex and lack internal coherence. They are texturally heterogeneous with grain sizes between ~5 and 30 mm. Psammite schollen vary from ovoid-lenses to blocky-rectangular shapes with low–moderate aspect ratios (e.g. see similar schollen in leucocratic diatexite in Fig. 4a). Pelite schollen contain a greater proportion of leucosomes, which include coarse-grained (~10–20 mm) idiomorphic K-feldspar and peritectic garnet.

Fine-grained (~2 mm) leucocratic domains comprise <10 vol.% of residual diatexites (Fig. 4b), and, where present, are interstitial between larger framework grains. Extremely residuum-rich domains locally develop cumulate-like textures (Fig. 4b), and this framework becomes dispersed in the more leucocratic domains. Cordierite ranges between ~5–10 mm and contains rounded inclusions of quartz, plagioclase, biotite, oxides, and zircon with yellow pleochroic halos as in the metatexites. Quartz films with cuspate terminations surrounds some cordierite, infilling the margin with adjacent corroded K-feldspar and biotite, indicating the former presence of melt (Fig 4e; Sawyer, 1999). These diatexites are interpreted to represent residual rocks that have lost a significant degree of melt (see Sawyer, 1998). Filtering of residuum from melt is supported by the transitional nature between residual and leucocratic diatexites at the outcrop scale (Fig. 4d).

*Leucocratic diatexites*

These diatexites are the most widespread, forming km-sized mappable units (Fig. 2) in the Grt-metatexite zone, and increase to the west in the Ovejeria complex. As in the residual diatexites, schollen are common (Fig. 4a). Pelite schollen tend to have higher aspect ratios in the leucocratic diatexites, and undergo greater *in situ* fragmentation than their psammitic counterparts. Margins between schollen and the granitic matrix are typically diffuse and become difficult to discern with increasing leucosome content in the schollen. Schollen are locally disaggregated into schlieren 5–30 cm long.

Biotite-rich schlieren are ubiquitous and vary from <1–5 cm wide, with a medium–coarse-grained lepidoblastic texture. Biotite within schlieren forms ~8 mm elongate, subhedral grains, and contains zircon inclusions surrounded by pleochroic halos. In contrast, isolated biotite in the diatexite is smaller (<4 mm long), typically anhedral with corroded margins and contains fewer included zircons. Disaggregation of schlieren into smaller biotite clots and isolated grains is visible in thin section.

Randomly dispersed garnets ~2–10 mm in diameter are typical, with occasional poikiloblasts intergrown with quartz up to ~40 mm. Garnet may be partly retrogressed to Bt+Qtz±Sil. Cordierite is similar to the residual diatexites, and commonly shows partial replacement along margins to tabular biotite (~7 mm), Qtz+Bt symplectites, fibrolitic sillimanite and sericite, with some reactions going to completion to produce subhedral cordierite pseudomorphs. It occurs typically within melanocratic domains, but can also be dispersed among more leucocratic parts of the diatexite. Orthopyroxene is less abundant than garnet and cordierite in the leucocratic diatexites. It forms subhedral grains ~5 mm in size, showing partial to complete retrogression. K-feldspar grains up to ~10 cm, large quartz grains up to ~5 cm, and aggregates of the two are isolated in granitic domains, and are interpreted to represent disruption of early pegmatite intrusions (e.g. Büttner *et al*.,

2005). These large K-feldspar grains have partially corroded margins, and contain small inclusions of rounded biotite, plagioclase, quartz, zircon, monazite and apatite. Leucocratic diatexites grade into schlieric granites (Fig. 4f), the most felsic rocks of the group with a relatively homogeneous appearance (Fig. 4c).

*Schlieric granites*

These rocks are more homogeneous versions of the leucocratic diatexites, containing less residual material (compare Figs. 4a and 4c). They are most common in the southwest part of the Ovejeria complex (Fig. 2), but also occur in the westernmost region of the Opx-metatexite zone of the Tolombón complex.

Schlieric granites are generally medium-grained (Fig. 4c) with a cargo of schollen generally comprising biotite, garnet, sillimanite, idiomorphic K-feldspar, cordierite, and, or, orthopyroxene, similar to the leucocratic diatexites. Subhedral to anhedral K-feldspar is smaller than in leucocratic diatexites (8–10 mm), and typically forms a dispersed framework with plagioclase, both feldspars containing rounded inclusions of quartz, biotite, and accessory zircon, monazite, and apatite. Interstitial material comprises anhedral quartz and fine-grained Qtz+Pl+Kfs+Bt. Large garnet crystals (20–30 mm diameter) are similar to those in the leucocratic diatexites. Cordierite in schlieric granites forms larger grains (10–40 mm), which are similarly inclusion-rich and variably altered. Schlieren are smaller in size (2–7 cm long) and have lower aspect ratios than in leucocratic diatexites.

**Felsic granitoids**

We divide these rocks into two groups based on mineralogy: tonalites and leucogranites, both of which show intrusive relationships with the host migmatites.

*Tonalites*

These are medium-grained (~5 mm), equigranular granitic rocks with 10–15 vol.% biotite (Figs. 5a, b). Their typical microstructure is characterised by blocky to rectangular plagioclase grains forming a framework connected at grain corners and edges with interstitial Qtz+Pl±Kfs±Bt±Sil (Fig. 5b), suggesting early plagioclase crystallisation forming a cumulate-like texture. Plagioclase is concentrically zoned with inclusions of rounded quartz, biotite, and elongate muscovite. Minor muscovite and sillimanite occur outside plagioclase, as well as small, fine-grained (<1 mm) biotite-rich schlieren with low aspect ratios (Fig. 5a). Minor orthopyroxene is typically heavily corroded, and partially replaced by biotite. Elongate, subhedral biotite is medium-grained (~2 mm long), and contains a high concentration of zircon inclusions surrounded by pleochroic halos, though a significant proportion of zircon and monazite are also included in quartz and plagioclase, and along grain margins. Tonalites intrude schists and metatexites in the Crd-subsolidus and Sil+Crd-metatexite zones of the Tolombón complex (Fig. 2), and form part of the composite Cafayate pluton along with leucogranites.

*Leucogranites*

Leucogranites are bodies ranging from metres to kilometres in size (Figs. 2, 5c–g), locally fed by metatexitic leucosomes at the outcrop scale (e.g. Fig. 3a, d). Larger bodies intrude metatexites and lower grade rocks of the Tolombón complex and comprise part of the Cafayate pluton. They are two-mica granites ranging from fine- to coarse-grained, with subhedral to anhedral plagioclase, quartz, and K-feldspar ~1.5–4 mm in fine-grained leucogranites, and ~5–15 mm in coarse samples, supported by interstitial Qtz+Kfs+Pl±Bt±Ms±Sil. Framework plagioclase crystals vary from euhedral to subhedral and are generally blocky to rectangular. Biotite grains have embayed and corroded margins,

are <0.7 mm long in fine leucogranites and up to 2 mm in coarse-grained samples, and comprise <5 vol.% of the rock. Most K-feldspar is subhedral to anhedral with irregular margins, and K-feldpsar phenocrysts, where present, contain inclusions of tabular to elongate biotite and rounded quartz and plagioclase. Schlieren are rare in leucogranites, and vary in composition from biotite-rich to muscovite-sillimanite-rich, sometimes surrounded by leucocratic rims (Fig. 5c). They have similar form to those in schlieric granites. Leucogranite bodies 1–5 m in diameter sometimes contain large garnet porphyroblasts (~30 mm; e.g. Fig. 3a) similar to leucocratic diatexites and schlieric granites. Smaller (<1–3 mm), subhedral and inclusion-free magmatic garnet is present in larger intrusive leucogranites (Fig. 5c, arrow). Roughly equant clots of sericite, biotite, and sillimanite ~0.5–3 mm long are taken to represent pseudomorphs after cordierite.

Pink granites are a subset of leucogranite rich in K-feldspar that intrude both the Tolombón and Ovejeria complexes. They may contain small modal contents of Sil±Grt±Crd and little, if any, plagioclase. Intrusions into Tolombón complex metatexites are generally medium-grained (~5 mm), and contain cordierite or garnet ~5–15 mm in size (Fig. 5d, e). In contrast, intrusions of pink granite into diatexites of the Ovejeria complex are coarse-grained (~10–20 mm; Figs. 5f, g) with larger garnet porphyroblasts up to ~40 mm in diameter partly retrogressed to form nodules of Grt+Bt+Sil+Qtz (Fig. 5g). They have irregular margins with diatexites, where individual coarse grains protrude into, or are isolated within the diatexite (arrows in Fig. 5f).

## ACCESSORY PHASES

As previously mentioned, the dominant accessory phases present in the Sierra de Quilmes migmatites and granites are zircon, monazite, and apatite. Here, we briefly describe the

textures of these main accessory phases, and their variation between the different rock types.

Zircons generally fall into three broad morphological types based on aspect ratio (AR): stubby (AR ~1:1–2), prismatic (AR ~1:3), and elongate (AR >1:4). In the metatexites, zircons are generally stubby, sometimes with rounded grain margins, whereas diatexites and schlieric granites contain a roughly equal mixture of all morphological types (e.g. Figs. 6a, b). They are most prevalent in melanocratic domains of the migmatites. In the felsic granitoids, zircon grains are typically prismatic and overall less abundant compared with the migmatites and schlieric granites.

Across all migmatites and granites, monazite typically varies from blocky to hexagonal (e.g. Fig. 6c), sometimes with rounded grain margins. However, in the metatexites, monazite can also form very small (<10 μm), parasitic grains crystallised on the margins of corroded apatite (e.g. Fig. 6d). As with zircon, the majority of monazite is generally found within melanocratic zones of the migmatites and is comparatively less abundant in the felsic granitoids.

Apatite generally forms blocky to rounded grains, sometimes with corroded margins as described above (e.g. Fig. 6d), and is most common in the metatexites. In contrast to zircon and monazite, apatite is abundant in both leucocratic and melanocratic domains within the migmatites.

## GEOCHEMISTRY

Here we group residual metatexites and residual diatexites together as residual migmatites, and leucocratic metatexites and leucocratic diatexites as leucocratic migmatites, based on

the above descriptions. Schlieric granites are separated from leucocratic diatexites based on their relatively homogeneous field appearance and lower ferromagnesian mineral content. Felsic granitoids are sub-divided as above. New whole-rock geochemical analyses were acquired for a suite of five Puncoviscana Formation (metasedimentary) samples, four residual migmatites, six leucocratic migmatites, five schlieric granites, ten leucogranites, including five pink granites, and one tonalite (Table 1). Large samples (3–5 kg) were collected to account for heterogeneity and provide an accurate representation of outcrops. For diatexites, the most homogeneous sections with minimum amounts of schollen were collected. All analysed samples comprise fresh and well-preserved assemblages. General mineralogy and grainsize of the migmatites sampled are as described above (see Supplementary Data Electronic Appendix 1 for specific sample information). Results were analysed in combination with existing whole-rock data from the Sierra de Quilmes reported in Finch *et al*. (2015; Supplementary Data Electronic Appendix 2) complemented with existing geochemical analyses of leucogranitic rocks (*sensu lato*) from the northeast Sierra de Quilmes from Rapela (1976), Rapela & Shaw (1979), Becchio *et al*. (1999), and Lucassen *et al*. (2001), and from the Sierra de Molinos further north (Sola *et al*., 2013).

Between 2 and 3 kg of each sample was jaw crushed with splits pulverised in a tungsten-carbide mill. Major element analyses for the new samples was conducted at the Australian Research Council Centre of Excellence in Ore Deposits (CODES), University of Tasmania, Australia, on a Panalytical Axios Advanced 4.0 kW X-ray Fluorescence (XRF) Spectrometer. Trace element analyses of six samples were obtained at the University of Melbourne, Victoria, Australia, using dissolution ICP-MS. For most trace elements of the remaining samples, dissolution ICP-MS was conducted at Monash University, Victoria, Australia, while Zr was analysed via XRF at CODES, University of Tasmania. Details of the analytical procedures are provided in Supplementary Data Electronic Appendix 3.

We have compared this broad data set on anatectic rocks (migmatites and granitic rocks) with geochemical data for the lower-grade, unmelted Puncoviscana Formation given in Table 1 (5 new samples) and Supplementary Data Electronic Appendix 4 (from Lucassen *et al*., 2001; Do Campo & Guevara, 2005; Zimmermann, 2005; Sola *et al*., 2013). The Puncoviscana Formation protolith is plotted as grey fields in figures and comprise 156 samples (5 new and 158 existing analyses, with seven outliers removed). These rocks range in silica content from 51 to 88 wt %; most psammites and pelites have an aluminium saturation index (ASI) >1 (Fig. 7a). Silica is negatively correlated with $FeO_T$ + MgO (Fig. 7b), $K_2O$ (Fig. 7c), $TiO_2$, and $Al_2O_3$ (not shown), attributed to the compositional maturity of the sediments (Pettijohn *et al*., 1972). The Puncoviscana Formation is LREE-enriched, and concentrations between samples span approximately one order of magnitude.

Migmatites and granites are also peraluminous with ASI ranging from 1.10–3.41 (Fig. 7a). Major element plots reveal multiple negative trends for $FeO_T$ + MgO across different rock types, one parallel to the Puncoviscana Formation comprising mostly of leucocratic migmatites and schlieric granites, and another, steeper trend linking pure biotite to the felsic granitoids through a number of residual migmatites (Fig. 7b).

$K_2O$ forms an ill-defined negative correlation with $SiO_2$ for the migmatites and schlieric granites (Fig. 7c). In contrast, the felsic granitoids show a steep positive trend from tonalites with only ~1.3 wt % $K_2O$ at ~73 wt % $SiO_2$, through leucogranites to pink granites with >5 wt % $K_2O$ at ~75 wt % $SiO_2$ (arrow in Fig. 7c). The same steep trend can be seen in data from other leucogranitic rocks in the region. Two experimental melt compositions for pelites from the Himalayas (MBS and MS, Fig. 7c; Patiño Douce & Harris, 1998) plot along the same trend. The compositional difference between tonalites and leucogranites, especially pink granites, is highlighted in the plot of $K_2O$ vs. CaO + $Na_2O$ (Fig. 7d): tonalites plot in the lower right CaO + $Na_2O$-rich, $K_2O$-poor end, consistent

with high modal plagioclase, whereas pink granites define a trend towards $K_2O$-rich and $CaO + Na_2O$-poor, consistent with high K-feldspar contents.

A plot of $FeO_T + MgO$ vs. $K_2O$ (Fig. 8) is particularly useful in determining processes of migmatite evolution and anatectic granite formation from metasedimentary protoliths (e.g. Sawyer, 1998; Milord *et al*., 2001), because peritectic phases resulting from typical dehydration melting reactions plot in different quadrants of the diagram. The residual migmatites define a broad spread in $K_2O$ at the high $FeO_T + MgO$-rich end of the plot, between the Grt-Crd-Opx and Bt vectors (Fig. 8), consistent with the high modality and wide variation of ferromagnesian phases between outcrops. Leucocratic migmatites and schlieric granites range between ~3.8 and 9 wt % $FeO_T + MgO$, and plot on top of the field defined by the Puncoviscana Formation (Fig. 8). The spread in $K_2O$ of the leucocratic migmatites is similar to that for residual migmatites, whereas the schlieric granites define a slightly more restricted range.

In contrast, the felsic granitoids form a band between ~0 and 3.8 wt % $FeO_T + MgO$ below the Puncoviscana Formation protolith field (Fig. 8), but with a wide spread of $K_2O$. Tonalites plot in the lower left quadrant towards the Qtz-Pl vector, whereas pink granites plot on the opposite side in the lower right quadrant towards the Kfs-Ms vector (Fig. 8). The trend within these rocks is reinforced by data from other leucogranitic rocks in the region, and includes the two experimental melts from Patiño Douce & Harris (1998).

*Trace elements*

Trace element concentrations were plotted as a function of $FeO_T + MgO$ (Fig. 9) to determine trace element behaviour relative to melt and residuum. Of particular interest are $LREE_T$, Th, Zr, and U, which relate to the mobilization of accessory minerals, including monazite and zircon (Bea, 1996), and the transfer of the heat-producing elements Th and U

with magmas through the crust. The plots can be divided into two sections with distinct behaviours above and below $FeO_T$ + MgO = 3.8 wt % (roughly the limit between felsic granitoids and other rock types in Fig. 8). Above this value, migmatites and most schlieric granites lack an obvious trend with increasing $FeO_T$ + MgO. Below, felsic granitoid samples show a systematic drop in $LREE_T$, Th, and Zr with decreasing $FeO_T$ + MgO, suggesting a decrease in the accessory minerals monazite and zircon compared to the source. The felsic granitoids are undersaturated in Zr (saturation line in Fig. 9c; Boehnke *et al*., 2013), and the majority are undersaturated with respect to LREE (saturation line in Fig. 9a; Rapp & Watson, 1986). The correlation between U and $FeO_T$ + MgO is ill defined (Fig. 9d), and values for all migmatites and granites range between 0.45 and 4.6 ppm U with one residual metatexite at 6.2 ppm. The average is 2.3 ppm, slightly below upper crustal values of 2.7 ppm. We interpret this complexity to reflect different behaviours of various U-bearing accessory minerals during melting (e.g. Bea, 2012). Trace element trends for felsic granitoids are echoed by existing data for the other leucogranitic rocks (Fig. 9).

Residual and leucocratic migmatites show broadly similar REE patterns in chondrite-normalised plots (Figs. 10a, b), both being LREE-enriched. HREE patterns are generally weakly to moderately depleted and display the most variation of all rock types ($[La/Yb]_N$: ~1–112). One residual migmatite (SQ119b) displays a strongly HREE-enriched pattern (Fig. 10a), reflecting its high modal proportion of garnet that is similarly indicated by high MnO and Y compared to the rest of the suite (see Table 1). Schlieric granites (Fig. 10c) display a narrower range of REE compared to the migmatites ($[La/Yb]_N$: ~9–39), and plot almost on top of the Puncoviscana Formation field.

Felsic granitoids tend to be impoverished in REE compared to the Puncoviscana Formation (Figs. 10d–f), in accordance with their generally low $LREE_T$, Th, and Zr contents (Fig. 9). Their profiles are LREE-enriched, with flat to weakly enriched or

depleted HREE patterns ($[La/Yb]_N$: ~2–54). The tonalite samples both display moderate REE concentrations (Fig. 10d), whereas absolute REE concentrations among leucogranites vary by approximately one order of magnitude (Figs. 10e, f).

## DISCUSSION

Granites define a wide compositional spectrum compared to that predicted by experimental melts. This has important implications for the chemical differentiation and stabilisation of the crust. Since the restite unmixing model of White & Chappell (1977), there has been extensive discussion regarding the entrainment of residuum in anatectic melts (e.g. Chappell *et al*., 1987; Sawyer, 1994, 1998; Milord *et al*., 2001; Guernina & Sawyer, 2003; Stevens *et al*., 2007; Dorais & Spencer, 2014; Carvalho *et al*., 2016). Restite unmixing, involving complete mobilisation of the source followed by gradual filtering of residuum (White & Chappell, 1977), and peritectic assemblage entrainment (PAE), where extreme filtering allows mobilisation of only the smallest peritectic grains and accessory phases (Stevens *et al.*, 2007; Taylor & Stevens, 2010), represent two end-members of residuum entrainment. Here we will show how migmatites and granites in the Sierra de Quilmes define two intermediate behaviours between these end-members that accounts for the compositional range of granites. Firstly, we demonstrate the genetic link between migmatites and the various granites based on their field relationships. We then detail two contrasting styles of granite-forming processes: (a) the Tolombón style, marked by efficient melt segregation and extraction from the source; (b) the Ovejeria style, associated with mobilisation of residuum in diatexites. We then explore the behaviour of accessory minerals relative to the different styles of granite formation, and discuss the implications for elemental distribution during crustal melting.

## The migmatite–granite link

A genetic relationship between the migmatites and various granites can be directly observed from their field relations. Here, we present a number of lines of evidence indicating that the migmatites are the source of the various granites.

The studied region provides excellent exposure of a tilted anatectic complex to approximate depths of 20 km (i.e. maximum pressures of ~6 kbar; Büttner *et al*., 2005). As previously mentioned, migmatitic leucosomes feed into larger pools of homogeneous leucocratic granite at outcrop scale (Figs. 3a, d). The same can be translated to the larger scale, where plutons can be traced back to the source, defining similar patterns at the map scale. The granitic bodies are either rich in schollen of the metasedimentary source, or are otherwise leucocratic (e.g. the Cafayate pluton, Fig. 2). In all cases, the granites also have a typical mineralogy linking them to the source, containing one or several of the following minerals: muscovite, sillimanite, garnet, cordierite or orthopyroxene. Furthermore, basaltic intrusions or I-type granites are absent, and there is no evidence suggestive of previous mingling with I-type magmas, such as mafic microgranular enclaves (MMEs), or hornblende, or titanite in any magmatic rocks from the region mapped. This suggests that all the magmatic rocks are derived from the metasedimentary pile, a conclusion supported by similar high-T rocks from the Sierra de Molinos, ~100 km north of Sierra de Quilmes along strike, which reveal a similarity in isotopic composition between migmatites, leucogranites, and the Puncoviscana Formation (Sola *et al*., 2013).

## Styles of granite formation

*Tolombón style: efficient melt segregation, minor residuum entrainment*

Leucosomes begin to segregate once sufficient melt is available to form an interconnected network (e.g. ~7 vol.%; Rosenberg & Handy, 2005), and represent partly preserved melt

extraction pathways (e.g. Brown *et al*., 1995; Reichardt *et al*., 2010). This is directly observed at the outcrop scale in the Sierra de Quilmes metatexites where leucosomes feed into homogeneous leucogranite pools (e.g. Fig. 3d). We define the Tolombón style of granite formation, where melt extracted from metatexites is relatively filtered and carries little residual material.

Strongly residual metatexites comprise up to ~90 vol.% ferromagnesian minerals with only thin, remnant leucosomes (Fig. 3e). These rocks are complemented by felsic granitoids comprising <10 vol.% ferromagnesian minerals (Fig. 5). The loss of melt from metatexites is also evidenced by collapse structures (Fig. 3c; Marchildon & Brown, 2003), small leucosome volume compared to peritectic mineral size (e.g. Fig. 3e), and limited retrogression of peritectic minerals (Fig. 3f; White & Powell, 2002). The low biotite content (<3 vol.%) of leucosomes, and the tendency for peritectic minerals to remain in the residuum (Figs. 3e, 4b), imply efficient melt extraction away from the solids. These observations are further supported by the complementary composition of the residual migmatites and felsic granitoids, schematically represented in Fig. 11: the compositional field of residual migmatites plots opposite that of the felsic granitoids, and the filtering of residuum denoted by the shaded arrow culminates in leucogranites with similar compositions to experimentally produced melts (MBS and MS in Fig. 11).

Efficient filtering of melts from solids is further supported by the zircon U-Pb geochronology of one pink granite (sample marked in Fig. 9c; unpublished data). This sample lacks detrital Puncoviscana Formation ages in contrast with the schlieric granites (three samples investigated), which contain high proportions (up to ~90%) of detrital zircon.

*Ovejeria style: rock disaggregation, major residuum entrainment*

Diatexites have lost coherence and are able to flow *en masse* (Brown, 1973), preventing the extraction of 'pure' melts (Sawyer, 1994). The Ovejeria style approaches the restite unmixing model proposed by White & Chappell (1977), and corresponds to the gradual and inefficient separation of melt from residuum during flow of diatexites. This process is recorded by the imperfect filtering and gradual changes between residual and leucocratic diatexites and schlieric granites (Fig. 4). These granitic rocks are comparatively rich in ferromagnesian components, and their composition would more closely image the source than the Tolombón style of melt extraction. In detail, the slightly lower $FeO_T$ + MgO of schlieric granites reflects the lower residuum content compared with leucocratic migmatites (Fig. 11). It is possible that some residue-poor melt may have resulted from *en masse* flow segregation to produce compositions similar to the felsic granitoids of the Tolombón style, locally producing residual diatexites.

*Fractionation*

The spread defined by the Tolombón-style felsic granitoids in Figs. 8 and 11 suggests melt fractional crystallisation defining a trend linking high CaO + $Na_2O$ tonalites to high $K_2O$ pink granites, through leucogranitic compositions generated by dehydration melting experiments with similar protolith compositions (e.g. MBS and MS in Figs. 8 and 11; Patiño Douce & Harris, 1998). These experimental melts are of Himalayan Ms±Bt schists after pelites with comparable compositions to the Puncoviscana Formation. Experiments were run at 6 kbar, and 750 (MBS) and 800 °C (MS; Patiño Douce & Harris, 1998), similar to the estimated peak P-T conditions of ~6 kbar and 800 °C for the Sierra de Quilmes (Büttner *et al*., 2005). Biotite dehydration in variable metasedimentary protoliths, such as the Puncoviscana Formation (e.g. Fig. 8), produces a relatively limited range of

experimental melt compositions (e.g. Figs. 2 & 3 in Gao *et al.*, 2016), further supporting fractional crystallisation to explain the chemical trend of the felsic granitoids.

Carvalho *et al*. (2016) demonstrated that plagioclase crystallised first from the anatectic melt, producing a dense framework of accumulated crystals, similar to our tonalites (see Fig. 5b). This microstructure, coupled with the low $K_2O$ contents of tonalites (e.g. Figs. 7c, d), is consistent with early plagioclase crystallisation and removal of an evolved melt from the interstices. Early crystallisation in the tonalites is further supported by the framework texture of plagioclase, connected at grain corners and edges, with interstitial quartz and, where present, K-feldspar. At the other compositional end of the felsic granitoid trend, pink granites are rich in $K_2O$, poor in $CaO + Na_2O$ (e.g. Figs. 7c, d), and are interpreted to represent the evolved melt (e.g. Carvalho *et al*., 2016). Although the Ovejeria style is defined by inefficient separation of melt from residuum, local compositional variations indicate some restite unmixing (White & Chappell, 1977), and plagioclase and K-feldspar fractionation possibly contributes to the wide range of $K_2O$ and $CaO + Na_2O$ among the leucocratic migmatites and schlieric granites (Figs. 7d & 8). However, as mentioned above, chemical variation associated with the Ovejeria style strongly reflects the wide range of protolith compositions (e.g. Fig. 8).

**Magma migration**

Ovejeria-style granite formation is only observed within the highest temperature zones outcropping in the west of Sierra de Quilmes (Fig. 2). There is no evidence to suggest that diatexitic magmas were transported far from their source, implying locally restricted magmatic flow. In order to form diatexites, melt must accumulate in the source, possibly reflecting weak pressure gradients driving melt extraction. This same reason, together with

the high viscosity and density of a magma loaded with solids, could explain why diatexites remained close to their source.

In contrast, the Tolombón-style, prevalent in the east, must have been associated with a higher pressure gradient that contributed to continuous melt extraction from metatexites. This formed felsic granitoids both close to the site of melting (e.g. Fig. 3a), and at higher crustal levels, including the Cafayate pluton that intruded the Sil+Crd-metatexite zone (Fig. 2) at estimated *P–T* conditions of ~650 °C and 3.6 kbar (Büttner *et al*., 2005), ~9 km above their source at ~6 kbar.

**Behaviour of accessory phases**

Accessory minerals (e.g. zircon, monazite, apatite, and titanite) typically host most of the U, Th, Zr, Y, Hf, and REE in granites (Bea, 1996). Their fate during anatexis plays a major role in the distribution of these trace elements within the continental crust, and can be tracked through trace element behaviour during partial melting and granite evolution.

As described earlier, the Sierra de Quilmes accessory mineral assemblage is dominated by zircon, monazite, and apatite, with minor xenotime. Zircons host a large proportion of the Zr in peraluminous granites and associated crustal source rocks, and typically contain a third of the total U (Bea, 1996). Most of the remaining U is hosted by either monazite or xenotime depending on the whole-rock composition (Bea, 1996). Monazite also hosts ~70–80 wt % of the LREE, followed by apatite (~14–19 wt %), and contains ~65–80 wt % of the total Th (Bea, 1996). We therefore take Zr trends to represent zircon behaviour during anatexis, and both LREE and Th trends to chiefly represent monazite.

The lack of a trend in $LREE_T$, Th, and Zr contents in all rock types with $FeO_T$ + MgO >3.8 wt % (Figs 9a–c) suggest that Ovejeria-style magma formation was inefficient

in either concentrating or diluting accessory minerals. This contrasts with more leucocratic rocks ($FeO_T$ + MgO <3.8 wt %), which define a positive trend between these trace elements and $FeO_T$ + MgO. The remaining discussion focuses on the Tolombón-style felsic granitoids.

The composition of magmatic rocks in terms of Zr, $LREE_T$, Th, and U depends on the ability of the melt to carry or dissolve inherited grains of zircon and monazite. Our unpublished results on zircon dating of felsic granitoids show a lack of inherited grains, suggesting relatively clean melt segregation with few accessories. Accessory mineral dissolution during anatexis depends on multiple related factors including *P–T* conditions (Roberts & Finger, 1997; Kohn *et al*., 2015), melt composition (Watson & Harrison, 1983; Wolf & London, 1995) and water content (e.g. Rapp & Watson, 1986; Stepanov *et al*., 2012), kinetics of melting reactions (Harrison & Watson, 1983; Rapp & Watson, 1986), the rate of metamorphic processes (Watt *et al*., 1996), textural location of individual grains (Watson *et al*., 1989) and crystal size distribution (Watson, 1996). Early experimental and observational data (e.g. Watson & Harrison, 1983; Rapp & Watson, 1986; Rapp *et al*., 1987; Watt & Harley, 1993; Wolf & London, 1995) predict that the peraluminous melts produced at peak Famatinian conditions of ~800 °C and 6 kbar (Büttner *et al*., 2005) would be inefficient at dissolving zircon, monazite, and xenotime, but would be efficient in dissolving apatite. The compositions of the Tolombón-style felsic granitoids support these predictions. We use whole-rock trace element geochemistry to first examine the behaviour of zircon and then discuss the fate of monazite and apatite during anatexis. Because xenotime is present in very minor amounts, its low modal abundance and limited solubility in peraluminous melts (Wolf & London, 1995) suggests a negligible impact on trace elements.

*Zircon*

The depletion of Zr (thus zircon) in the felsic granitoids relative to the residual migmatitic source (Fig. 9c) confirms that zircon dissolution during melting was limited. Zircon solubility increases with increasing temperature and water content of the melt (Harrison & Watson, 1983) and is comparably low for peraluminous compositions (Watson & Harrison, 1983). The apparent limited dissolution of zircon could therefore be due to melt aluminosity (e.g. Fig. 7a) and suggests relatively dry compositions.

Zirconium saturation in peraluminous magmas from 750–850 °C is ~140–340 ppm, and is specifically estimated at ~224 ppm for ~800 °C (Fig. 9c; see Fig. 7a in Boehnke *et al*., 2013). However, the Sierra de Quilmes felsic granitoids have generally lower Zr concentrations ranging from 14–173 ppm (Table 1 & Fig. 9c). For pelitic protoliths, it is expected that the melts will become saturated in Zr before all zircons are dissolved (Kohn *et al*., 2015), especially for concentrations ≥100 ppm of Zr in the source (Watson & Harrison, 1983; Yakymchuk & Brown, 2014). The Puncoviscana Formation sedimentary rocks have an average Zr concentration of ~231 ppm (Fig. 9c, Supplementary Data Electronic Appendix 4), and are therefore expected to produce zircon-saturated melts. Given that the suite of felsic granitoids includes rocks ranging from cumulates through rocks representing melt compositions to fractionated end-members, this implies that the Tolombón style melts did not achieve Zr saturation prior to extraction, an important consideration for zircon saturation thermometry.

Zirconium undersaturation implies one of three possible explanations: (1) that zircons in the source were sequestered as inclusions in stable phases during melting, or in anhydrous peritectic minerals formed through melting reactions (e.g. Grt, Crd, Opx), rendering them unavailable; (2) melts were extracted before equilibration with the source (e.g. Watt & Harley, 1993); or (3) predictions of Zr saturation values are overestimated for

dry and peraluminous melt compositions. The majority of zircons in mesosomes are contained in quartz, feldspar, or biotite, or situated along grain margins, therefore potentially exposed to the melt during anatexis. We are unable to further constrain whether equilibrium has been achieved with the source, but have no arguments to support fast melt mobilisation.

*Phosphates*

The felsic granitoids are depleted in LREE and Th compared with the more mafic rock groups (Figs. 9a, b), indicating limited monazite dissolution during melting. This disagrees with the findings of Yakymchuk & Brown (2014), who predicted that most monazite, if not all, should dissolve during dehydration of metasedimentary protoliths, possibly reflecting an absence of apatite. However, as for zircons, other experimental studies predict low monazite solubility in peraluminous melts (Montel, 1986; Rapp *et al*., 1987), which only increases with rising temperature and water content (Rapp & Watson, 1986; Stepanov *et al*., 2012).

Monazite solubility experiments suggest that granitic melt containing ~6 wt % $H_2O$ at 800 °C will reach monazite saturation at LREE values of ~300 ppm (see Fig. 6 in Rapp & Watson, 1986). Estimating monazite solubility for granitic melt containing 4 wt % $H_2O$ (minimum melt $H_2O$ content at ~800 °C and 6 kbar; see Fig. 2 in Holtz & Johannes, 1994) gives an LREE saturation value of ~150 ppm at ~800 °C (indicated in Fig. 9a; see Fig. 6 in Rapp & Watson, 1986). This range extends from ~125–250 ppm LREE for 750–850 °C melts (Rapp & Watson, 1986), using relevant minimum water contents of 6 and 3 wt %, respectively (Holtz & Johannes, 1994). The Puncoviscana Formation protolith has an average $LREE_T$ concentration of ~238 ppm (Fig. 9a; Supplementary Data Electronic Appendix 4), and the migmatites ~195 ppm (Fig. 9a). As was the case with Zr, this suggests

that the protolith contained sufficient LREE to saturate the melt. However, only three felsic granitoid samples (one each of tonalite, leucogranite, and pink granite) have $LREE_T$ concentrations approximating the expected value of ~150 ppm for monazite saturation at 800 °C (Fig. 9a; Rapp & Watson, 1986). The remaining samples all contain <100 ppm $LREE_T$, and therefore formed from monazite-undersaturated melts.

The fate of monazite, therefore LREE and Th, is also tied to that of apatite during anatexis. Apatite dissolution is favoured by strongly peraluminous melt compositions, rising by a factor of 10 with melt ASI increasing from 1.1 to 1.2 (Wolf & London, 1995). Apatite typically contains ~14–19 wt % of the total LREE in peraluminous granites and associated crustal sources (Bea, 1996); apatite dissolution will release these, as well as considerable P, into the melt. However, the maximum $P_2O_5$ solubility of monazite and xenotime in peraluminous melt is limited to <0.05 wt % (Wolf & London, 1995). The felsic granitoids contain >0.06 wt % $P_2O_5$ (see Table 1 and Supplementary Data Electronic Appendix 2), suggesting that the extracted melt was saturated in P with respect to these phosphates, most likely resulting from efficient apatite dissolution. Therefore, preferential apatite dissolution contributed sufficient P to stabilize monazite and xenotime in the peraluminous melts (Wolf & London, 1995), thus restricting the amount of LREE and Th added to the melt through monazite dissolution. Apatite dissolution in some Sierra de Quilmes metatexites, indicated by corroded apatite margins with crystallisation of tiny monazite crystals on the surfaces of dissolving grains (e.g. Fig. 6d), is interpreted to result from oversaturation of LREE in an enriched boundary layer of melt (Wolf & London, 1995).

*Controls on U*

The trend for U revealed by the felsic granitoids is undefined, varying widely and independently of $FeO_T$ + MgO. Uranium is hosted by multiple accessory phases in peraluminous granites and associated source rocks: for an ASI >1.15, zircon can contain up to one third and monazite up to two thirds of the total U (Bea, 1996). Uranium is weakly positively correlated with Th among the felsic granitoids (dashed line, Fig. 12a), but shows no trend with Zr (Fig. 12b). This may be reflecting the presence of Th and U in both zircon and monazite.

The poor solubility of monazite, zircon and xenotime in peraluminous, relatively dry melts should lead to U behaving compatibly and being depleted in the felsic granitoids. However, the U content of these granites overlaps with that of the other rock groups, including the Puncoviscana Formation source (grey field in Fig. 12). This suggests further complexity in the controls of U distribution, probably resulting from three overlapping factors: dissolution of U-rich apatite into the melt; a heterogeneous melt source in terms of accessory mineralogy, as well as initial U, Th, and Zr contents as demonstrated by the grey fields in Fig. 12; fractionation of accessory phases in the evolving felsic granitoids with the pink leucogranites having very low values of these trace elements.

## Implications for crustal differentiation

The deep continental crust is typically depleted in incompatible elements, including the heat-producing elements, relative to the bulk continental crust (Hacker *et al*., 2015), which is important for the thermal and mechanical stabilisation of the lower crust and lithosphere (Sandiford & McLaren, 2006). Granitic rocks, chiefly concentrated in the upper continental crust (UCC), are characteristically enriched in incompatible elements (Kemp & Hawkesworth, 2003; Sandiford & McLaren, 2006). This typical crustal differentiation

occurs primarily in magmatic arc settings, where new continental crust is generated through fractional crystallisation or remelting of a mantle-derived basaltic source (Kemp & Hawkesworth, 2003).

Although dehydration melting of the continental crust can produce large volumes of melt (e.g. Patiño Douce & Johnston, 1991), the resulting granites do not always share the enrichment of trace elements typical of the UCC (Sawka & Chappell, 1986; Bea, 2012), and are therefore unlikely to drive typical crustal differentiation (Kemp & Hawkesworth, 2003). For example, Sawka & Chappell (1986) found that peraluminous S-type granites from the Lachlan Fold Belt had lower U and Th concentrations than their residual source rocks. Such granites, depleted in incompatible trace elements, are unlikely to drive typical crustal differentiation (Kemp & Hawkesworth, 2003). In the Sierra de Quilmes, the strongly peraluminous melts produced by biotite dehydration are incapable of dissolving large quantities of accessory minerals, such as zircon and monazite, which host the majority of the Zr, LREE, Th, and a significant fraction of the U, in such high-grade crustal rocks (Bea, 1996). The felsic granitoids in this study are generally depleted in these trace elements relative to the average UCC (leucogranite field in Fig. 13), or relative to the Puncoviscana Formation (not shown), whereas the residual migmatites (Fig. 13) as well as leucocratic diatexites (not shown) are enriched. Schlieric granites have trace element patterns intermediate between those of leucogranites and residual migmatites and diatexites (Fig. 13), compositionally similar to the average UCC. However, the tendency for these magmas loaded with solids to remain in the source in the Sierra de Quilmes precludes their contribution to the upper crust. We conclude that melting of the Puncoviscana Formation in the Sierra de Quilmes, as an example of crustal granite generation, had the opposite effect to typical crustal differentiation by concentrating trace elements generally considered incompatible in the residual lower crust.

## CONCLUSIONS

We have defined two modes of granite magma formation in the Sierra de Quilmes. The Ovejeria style gives rise to diatexites, defining a group of rocks with broadly coincident compositions to the metasedimentary protolith. These rocks represent near-complete mobilisation of residuum, similar to the restite unmixing model originally proposed by White & Chappell (1977). Subsequent filtering and fractionation by *en masse* flow led to a rich range in rocks from residual to granitic diatexites, all of which seem to remain close to the source.

The Tolombón style is characterised by melt extracted from metatexites, with leucosomes feeding into felsic granitoids at higher crustal levels. These magmas were impoverished in trace elements typically considered incompatible, indicating efficient melt segregation with little entrainment of residuum. Upon cooling, the felsic granitoids underwent fractional crystallisation to produce a suite ranging from cumulate tonalites to evolved, K-feldspar-rich pink granites. Geochemical diversity of anatectic granites in the Sierra de Quilmes is therefore a function of the degree of residuum entrainment during melt extraction and subsequent fractionation during crystallisation.

Biotite dehydration melting produced dry, peraluminous melts which significantly influenced the solubility of the accessory phases. While the peraluminous nature of the melt favoured apatite dissolution, it was incapable of dissolving considerable amounts of zircon and monazite, explaining the low concentration of Zr, Th, LREE, and sometimes U, in the felsic granitoids. These elements therefore behaved compatibly and tended to stay in the source. The tendency for the Ovejeria-style granites, loaded with residuum, to remain close to the source, implies that neither the Ovejeria nor Tolombón style of granite formation was

capable of transferring these trace elements to the upper crust. We therefore conclude that, instead of contributing to typical crustal differentiation that enriches the upper continental crust in 'incompatible' trace elements, biotite dehydration melting of a metasedimentary protolith can have the opposite effect, concentrating these in the residual source, if there is no pressure gradient to drive extraction of residuum-rich magmas.

**FUNDING**

We gratefully acknowledge financial support from the Australian Research Council (grant DP110102543 to R.F.W.) and the Czech Science Foundation (grant P210-14-25995S to P.H.).

**ACKNOWLEDGEMENTS**

We thank M. Finch for help with sample preparation and compilation of existing literature. M. G. Fuentes and A. Ortiz are thanked for assistance during fieldwork, and M. Raveggi, J. Thompson, and A. Greig for their help with geochemical analyses. We thank M. Dorais and two anonymous reviewers for detailed and constructive reviews that helped improve the manuscript.

## REFERENCES


Aceñolaza, F. G., Miller, H. & Toselli, A. J. (1988). *The Puncoviscana Formation (Late Precambrian–Early Cambrian) – sedimentology, tectonometamorphic history and age of the oldest rocks of NW Argentina*. The Southern Central Andes, Lecture Notes in Earth Sciences **17**. Springer-Verlag, Berlin.

Acosta-Vigil, A., Buick, I., Cesare, B., London, D. & Morgan, G. B. (2012). The extent of equilibration between melt and residuum during regional anatexis and its implications for differentiation of the continental crust: A study of partially melted metapelitic enclaves. *Journal of Petrology* **53**, 1319-1356.

Adams, C. J., Miller, H., Aceñolaza, F. G., Toselli, A. J. & Griffin, W. L. (2011). The Pacific Gondwana margin in the late Neoproterozoic-early Paleozoic: Detrital zircon U-Pb ages from metasediments in northwest Argentina reveal their maximum age, provenance and tectonic setting. *Gondwana Research* **19**, 71-83.

Arzi, A. A. (1978). Critical phenomena in the rheology of partially melted rocks. *Tectonophysics* **44**, 173-184.

Bahlburg, H. (1998). *The geochemistry and provenance of Ordovician turbidites in the Argentine Puna*. In: Pankhurst, R. J., Rapela, C. W. (eds.) *The Proto-Andean Margin of Gondwana*, *Geological Society of London, Special Publications* **142**, 127-142.

Bea, F. (1996). Residence of REE, Y, Th and U in granites and crustal protoliths; implications for the chemistry of crustal melts. *Journal of Petrology* **37**, 521-552.

Bea, F. (2012). The sources of energy for crustal melting and the geochemistry of heat-producing elements. *Lithos* **153**, 278-291.

Becchio, R., Lucassen, F., Kasemann, S., Franz, G. & Viramonte, J. (1999). Geochemistry and isotope systematics of Early Paleozoic metamorphic rocks. Northwest Argentina and North Chile (21°-27°S). *Acta Geologica Hispanica* **34**, 273-299.

Bhadra, S., Das, S. & Bhattacharya, A. (2007). Shear zone-hosted migmatites (Eastern India): The role of dynamic melting in the generation of REE-depleted felsic melts, and implications for disequilibrium melting. *Journal of Petrology* **48**, 435-457.

Boehnke, P., Watson, E. B., Trail, D., Harrison, T. M. & Schmitt, A. K. (2013). Zircon saturation re-revisited. *Chemical Geology* **351**, 324-334.

Bons, P. D., Druguet, E., Castaño, L. M. & Elburg, M. A. (2008). Finding what is now not there anymore: Recognizing missing fluid and magma volumes. *Geology* **36**, 851-854.

Brown, M. (1973). The definition of metatexis, diatexis and migmatite. *Proceedings of the Geologists' Association* **84**, 371-382.

Brown, M. (2006). *Melt extraction from the lower continental crust of orogens: the field evidence*. In: Brown, M. & Rushmer, T. (eds.) *Evolution and differentiation of the continental crust*. Cambridge University Press UK, 331-383.

Brown, M. (2013). Granite: From genesis to emplacement. *Bulletin of the Geological Society of America* **125**, 1079-1113.

Brown, M., Averkin, Y. A., McLellan, E. L. & Sawyer, E. W. (1995). Melt segregation in migmatites. *Journal of Geophysical Research* **100**, 15,655-615,679.

Büttner, S. H., Glodny, J., Lucassen, F., Wemmer, K., Erdmann, S., Handler, R. & Franz, G. (2005). Ordovician metamorphism and plutonism in the Sierra de Quilmes metamorphic complex: Implications for the tectonic setting of the northern Sierras Pampeanas (NW Argentina). *Lithos* **83**, 143-181.

Carvalho, B. B., Sawyer, E. W. & Janasi, V. A. (2016). Crustal reworking in a shear zone: transformation of metagranite to migmatite. *Journal of Metamorphic Geology* **34**, 237-264.

Cawood, P. A. (2005). Terra Australis Orogen: Rodinia breakup and development of the Pacific and Iapetus margins of Gondwana during the Neoproterozoic and Paleozoic. *Earth-Science Reviews* **69**, 249-279.

Chappell, B. W., White, A. J. R. & Wyborn, D. (1987). The importance of residual source material (restite) in granite petrogenesis. *Journal of Petrology* **28**, 1111-1138.

Clemens, J. D. & Wall, V. J. (1981). Origin and crystallization of some peraluminous (S-type) granitic magmas. *Canadian Mineralogist* **19**, 111-131.

Coira, B., Kirschbaum, A., Hongn, F., Pérez, B. & Menegatti, N. (2009). Basic magmatism in northeastern Puna, Argentina: Chemical composition and tectonic setting in the Ordovician back-arc. *Journal of South American Earth Sciences* **28**, 374-382.

Dahlquist, J. A., Verdecchia, S. O., Baldo, E. G., Basei, M. A. S., Alasino, P. H., Urán, G. A., Rapela, C. W., Neto, M. C. & Zandomeni, P. S. (2016). Early Cambrian U-Pb zircon age and H-isotope data from the Guasayán pluton, Sierras Pampeanas, Argentina: implications for the northwestern boundary of the Pampean arc. *Andean Geology* **43**, 137-150.

DePaolo, D. J. (1981). Trace element and isotopic effects of combined wallrock assimilation and fractional crystallization. *Earth and Planetary Science Letters* **53**, 189-202.

Do Campo, M. & Guevara, S. R. (2005). Provenance analysis and tectonic setting of late Neoproterozoic metasedimentary successions in NW Argentina. *Journal of South American Earth Sciences* **19**, 143-153.

Dorais, M. J. & Spencer, C. J. (2014). Revisiting the importance of residual source material (restite) in granite petrogenesis: The Cardigan Pluton, New Hampshire. *Lithos* **202-203**, 237-249.

Finch, M. A., Weinberg, R. F., Fuentes, M. G., Hasalová, P. & Becchio, R. (2015). One kilometre-thick ultramylonite, Sierra de Quilmes, Sierras Pampeanas, NW Argentina. *Journal of Structural Geology* **72**, 33-54.

Finch, M. A., Weinberg, R. F. & Hunter, N. J. R. (2016). Water loss and the origin of thick ultramylonites. *Geology* **44**, 599-602.

Finch, M. A., Weinberg, R. F., Hasalová, P., Becchio, R., Fuentes, M. G. & Kennedy, A. (2017). Tectono-metamorphic evolution of the Famatinian Orogeny in the Sierra de Quilmes, Sierras Pampeanas, NW Argentina. *Geological Society of America Bulletin*.

Gao, P., Zheng, Y. F. & Zhao, Z. F. (2016). Experimental melts from crustal rocks: A lithochemical constraint on granite petrogenesis. *Lithos* **266-267**, 133-157.

Gardien, V., Thompson, A. B., Grujic, D. & Ulmer, P. (1995). Experimental melting of biotite + plagioclase + quartz ± muscovite assemblages and implications for crustal melting. *Journal of Geophysical Research* **100**, 15,581-15,591.

Guernina, S. & Sawyer, E. W. (2003). Large-scale melt-depletion in granulite terranes: An example from the Archean Ashuanipi subprovince of Quebec. *Journal of Metamorphic Geology* **21**, 181-201.

Hacker, B. R., Kelemen, P. B. & Behn, M. D. (2015). Continental lower crust. *Annual Review of Earth and Planetary Sciences* **43**, 167-205.

Harrison, T. M. & Watson, E. B. (1983). Kinetics of zircon dissolution and zirconium diffusion in granitic melts of variable water content. *Contributions to Mineralogy and Petrology* **84**, 66-72.

Holtz, F. & Johannes, W. (1994). Maximum and minimum water contents of granitic melts: implications for chemical and physical properties of ascending magmas. *Lithos* **32**, 149-159.

Hongn, F. D., Tubía, J. M., Aranguren, A., Vegas, N., Mon, R. & Dunning, G. R. (2010). Magmatism coeval with lower Paleozoic shelf basins in NW-Argentina (Tastil batholith): Constraints on current stratigraphic and tectonic interpretations. *Journal of South American Earth Sciences* **29**, 289-305.

Ježek, P., Willner, A. P., Aceñolaza, F. G. & Miller, H. (1985). The Puncoviscana trough - a large basin of Late Precambrian to Early Cambrian age on the pacific edge of the Brazilian shield. *Geologische Rundschau* **74**, 573-584.

Jordan, T. E. & Allmendinger, R. W. (1986). The Sierras Pampeanas of Argentina: a modern analogue of Rocky Mountain foreland deformation. *American Journal of Science* **286**, 737-764.

Jurewicz, S. R. & Watson, E. B. (1984). Distribution of partial melt in a felsic system: the importance of surface energy. *Contributions to Mineralogy and Petrology* **85**, 25-29.

Kelsey, D. E., Clark, C. & Hand, M. (2008). Thermobarometric modelling of zircon and monazite growth in melt-bearing systems: Examples using model metapelitic and metapsammitic granulites. *Journal of Metamorphic Geology* **26**, 199-212.

Kemp, A. I. S. & Hawkesworth, C. J. (2003). *Granitic Perspectives on the Generation and Secular Evolution of the Continental Crust*. In: Rudnick, R. L. (ed.) *The Crust* Vol. 3 *Treatise on Geochemistry* (eds. Holland, H. D. & Turekian, K. K.). Elsevier–Pergamon Oxford, 349-410.

Kohn, M. J., Corrie, S. L. & Markley, C. (2015). The fall and rise of metamorphic zircon. *American Mineralogist* **100**, 897-908.

Korhonen, F. J., Saito, S., Brown, M., Siddoway, C. S. & Day, J. M. D. (2010). Multiple generations of granite in the Fosdick Mountains, Marie Byrd Land, West Antarctica: Implications for polyphase intracrustal differentiation in a continental margin setting. *Journal of Petrology* **51**, 627-670.

Le Breton, N. & Thompson, A. B. (1988). Fluid-absent (dehydration) melting of biotite in metapelites in the early stages of crustal anatexis. *Contributions to Mineralogy and Petrology* **99**, 226-237.

Lucassen, F., Becchio, R., Harmon, R., Kasemann, S., Franz, G., Trumbull, R., Wilke, H. G., Romer, R. L. & Dulski, P. (2001). Composition and density model of the continental crust at an active continental margin - The Central Andes between 21° and 27°S. *Tectonophysics* **341**, 195-223.

Marchildon, N. & Brown, M. (2003). Spatial distribution of melt-bearing structures in anatectic rocks from Southern Brittany, France: Implications for melt transfer at grain- to orogen-scale. *Tectonophysics* **364**, 215-235.

McLennan, S. M., Taylor, S. R. & Hemming, S. R. (2006). *Composition, differentiation, and evolution of continental crust: constraints from sedimentary rocks and heat flow*. In: Brown, M. & Rushmer, T. (eds.) *Evolution and differentiation of the continental crust*. Cambridge University Press UK, 92-134.

Miller, C. F., Watson, E. B. & Harrison, T. M. (1988). Perspectives on the source, segregation and transport of granitoid magmas. *Transactions of the Royal Society of Edinburgh, Earth Sciences* **79**, 135-156.

Milord, I., Sawyer, E. W. & Brown, M. (2001). Formation of diatexite migmatite and granite magma during anatexis of semi-pelitic metasedimentary rocks: An example from St. Malo, France. *Journal of Petrology* **42**, 487-505.

Montel, J. M. (1986). Experimental determination of the solubility of Ce-monazite in $SiO_2$-$Al_2O_3$-$K_2O$-$Na_2O$ melts at 800°C, 2 kbar, under $H_2O$-saturated conditions. *Geology* **14**, 659-662.

Pankhurst, R. J., Rapela, C. W. & Fanning, C. M. (2000). Age and origin of coeval TTG, I- and S-type granites in the Famatinian belt of NW Argentina. *Transactions of the Royal Society of Edinburgh, Earth Sciences* **91**, 151-168.

Pankhurst, R. J., Rapela, C. W., Saavedra, J., Baldo, E., Dahlquist, J., Pascua, I. & Fanning, C. M. (1998). *The Famatinian magmatic arc in the central Sierras Pampeanas: an Early to Mid-Ordovician continental arc on the Gondwana margin*. In: Pankhurst, R. J., Rapela, C. W. (eds.) *The Proto-Andean Margin of Gondwana*, *Geological Society of London, Special Publications* **142**, 343-367.

Patiño Douce, A. E. & Harris, N. (1998). Experimental constraints on Himalayan anatexis. *Journal of Petrology* **39**, 689-710.

Patiño Douce, A. E. & Johnston, A. D. (1991). Phase equilibria and melt productivity in the pelitic system: implications for the origin of peraluminous granitoids and aluminous granulites. *Contributions to Mineralogy and Petrology* **107**, 202-218.

Pettijohn, F. J., Potter, P. E. & Siever, R. (1972). *Sand and sandstone*. Springer-Verlag, Heidelberg.

Piñan-Llamas, A. & Simpson, C. (2006). Deformation of Gondwana margin turbidites during the Pampean orogeny, north-central Argentina. *Geological Society of America Bulletin* **118**, 1270-1279.

Rapela, C. W. (1976). Las rocas granitoides de la region de Cafayate, provincia de Salta: aspectos petrologicos y geoquimicos. *Revista de la Asociacion Geologica Argentina* **31**, 26-278.

Rapela, C. W., Pankhurst, R. J., Casquet, C., Baldo, E., Saavedra, J., Galindo, C. & Fanning, C. M. (1998a). *The Pampean Orogeny of the southern proto-Andes: Cambrian continental collision in the Sierras de Cordoba*. In: Pankhurst, R. J., Rapela, C. W. (eds.) *The Proto-Andean Margin of Gondwana*, *Geological Society of London, Special Publications* **142**, 181-217.

Rapela, C. W., Pankhurst, R. J., Saavedra, J. & Galindo, C. (1998b). Early evolution of the proto-andean margin of South America. *Geology* **26**, 707-710.

Rapela, C. W. & Shaw, D. M. (1979). Trace and major element models of granitoid genesis in the Pampean ranges, Argentina. *Geochimica et Cosmochimica Acta* **43**, 1117-1129.

Rapela, C. W., Toselli, A., Heaman, L. & Saavedra, J. (1990). *Granite plutonism of the Sierras Pampeanas; An inner cordilleran Paleozoic arc in the southern Andes*. In: Kay, S. M. & Rapela, C. W. (eds.) *Plutonism from Antarctica to Alaska: Boulder, Colorado*. *Geological Society of America Special Paper* **241**, 77-90.

Rapela, C. W., Verdecchia, S. O., Casquet, C., Pankhurst, R. J., Baldo, E. G., Galindo, C., Murra, J. A., Dahlquist, J. A. & Fanning, C. M. (2016). Identifying Laurentian and SW Gondwana sources in the Neoproterozoic to Early Paleozoic metasedimentary rocks of the Sierras Pampeanas: Paleogeographic and tectonic implications. *Gondwana Research* **32**, 193-212.

Rapp, R. P., Ryerson, F. J. & Miller, C. (1987). Experimental evidence bearing on the stability of monazite during crustal anatexis. *Geophysical Research Letters* **14**, 307-310.

Rapp, R. P. & Watson, E. B. (1986). Monazite solubility and dissolution kinetics: implications for the thorium and light rare earth chemistry of felsic magmas. *Contributions to Mineralogy and Petrology* **94**, 304-316.

Regmi, K. R., Weinberg, R. F., Nicholls, I. A., Maas, R. & Raveggi, M. (2016). Evidence for hybridisation in the Tynong Province granitoids, Lachlan Fold Belt, eastern Australia. *Australian Journal of Earth Sciences* **63**, 235-255.

Reichardt, H., Weinberg, R. F., Andersson, U. B. & Fanning, C. M. (2010). Hybridization of granitic magmas in the source: The origin of the Karakoram Batholith, Ladakh, NW India. *Lithos* **116**, 249-272.

Roberts, M. P. & Finger, F. (1997). Do U-Pb zircon ages from granulites reflect peak metamorphic conditions? *Geology* **25**, 319-322.

Rosenberg, C. L. & Handy, M. R. (2005). Experimental deformation of partially melted granite revisited: Implications for the continental crust. *Journal of Metamorphic Geology* **23**, 19-28.

Rossi de Toselli, J. N., Toselli, A. & Toselli, G. (1976). Migmatizacion y metamorgismo en el basamento de la Sierra de Quilmes, al oeste de Colalao del Valle, Provincia de Tucuman, Argentina. *Revista de la Asociacion Geologica Argentina* **31**, 83-94.

Rudnick, R. L. & Gao, S. (2003). *The composition of the continental crust*. In: Rudnick, R. L. (ed.) *The Crust* Vol. 3 *Treatise on Geochemistry* (eds. Holland, H. D. & Turekian, K. K.). Elsevier–Pergamon Oxford, 1-64.

Sandiford, M. & McLaren, S. (2006). *Thermo-mechanical controls on heat producing distributions and the long-term evolution of the continents*. In: Brown, M. & Rushmer, T. (eds.) *Evolution and differentiation of the continental crust*. Cambridge University Press UK, 67-91.

Sawka, W. N. & Chappell, B. W. (1986). The distribution of radioactive heat production in I- and S-type granites and residual source regions: Implications to high heat flow areas in the Lachlan Fold Belt, Australia. *Australian Journal of Earth Sciences* **33**, 107-118.

Sawyer, E. W. (1991). Disequilibrium melting and the rate of melt-residuum separation during migmatization of mafic rocks from the Grenville front, Quebec. *Journal of Petrology* **32**, 701-738.

Sawyer, E. W. (1994). Melt segregation in the continental crust. *Geology* **22**, 1019-1022.

Sawyer, E. W. (1996). Melt segregation and magma flow in migmatites: Implications for the generation of granite magmas. *Transactions of the Royal Society of Edinburgh, Earth Sciences* **87**, 85-94.

Sawyer, E. W. (1998). Formation and evolution of granite magmas during crustal reworking: the significance of diatexites. *Journal of Petrology* **39**, 1147-1167.

Sawyer, E. W. (1999). Criteria for the recognition of partial melting. *Physics and Chemistry of the Earth, Part A: Solid Earth and Geodesy* **24**, 269-279.

Sawyer, E. W. (2008). *Atlas of Migmatites*. The Canadian Mineralogist, Special Publication 9. NRC Research Press, Ottawa, Ontario, Canada. 371 p.

Sims, J. P., Ireland, T. R., Camacho, A., Lyons, P., Pieters, P. E., Skirrow, R. G., Stuart-Smith, P. G. & Miró, R. (1998). *U-Pb, Th-Pb and Ar-Ar geochronology from the southern Sierras Pampeanas, Argentina: implications for the Palaeozoic tectonic evolution of the western Gondwana margin*. In: Pankhurst, R. J., Rapela, C. W. (eds.) *The Proto-Andean Margin of Gondwana*, *Geological Society of London, Special Publications* **142**, 259-281.

Sola, A. M., Becchio, R. A. & Pimentel, M. M. (2013). Petrogenesis of migmatites and leucogranites from Sierra de Molinos, Salta, Northwest Argentina: A petrologic and geochemical study. *Lithos* **177**, 470-491.

Solar, G. S. & Brown, M. (2001). Petrogenesis of migmatites in Maine, USA: Possible source of perluminous leucogranite in Plutons? *Journal of Petrology* **42**, 789-823.

Steenken, A., López de Luchi, M. G., Dopico, C. M., Drobe, M., Wemmer, K. & Siegesmund, S. (2011). The Neoproterozoic-early Paleozoic metamorphic and magmatic evolution of the Eastern Sierras Pampeanas: An overview. *International Journal of Earth Sciences* **100**, 465-488.

Stepanov, A. S., Hermann, J., Rubatto, D. & Rapp, R. P. (2012). Experimental study of monazite/melt partitioning with implications for the REE, Th and U geochemistry of crustal rocks. *Chemical Geology* **300-301**, 200-220.

Stevens, G., Villaros, A. & Moyen, J. F. (2007). Selective peritectic garnet entrainment as the origin of geochemical diversity in S-type granites. *Geology* **35**, 9-12.

Sun, S.-s. & McDonough, W. F. (1989). *Chemical and isotopic systematics of oceanic basalts: implication for mantle composition and processes*. In: Saunders, A. D., Norry, M. J. (eds.) *Magmatism in Ocean Basins* Vol. 42. *Geological Society London Special Publication*, 313-345.

Taylor, J. & Stevens, G. (2010). Selective entrainment of peritectic garnet into S-type granitic magmas: Evidence from Archaean mid-crustal anatectites. *Lithos* **120**, 277-292.

Thomas, W. A. & Astini, R. A. (2003). Ordovician accretion of the Argentine Precordillera terrane to Gondwana: A review. *Journal of South American Earth Sciences* **16**, 67-79.

Thompson, A. B. (1996). Fertility of crustal rocks during anatexis. *Transactions of the Royal Society of Edinburgh, Earth Sciences* **87**, 1-10.

Tindle, A. G. & Pearce, J. A. (1981). Petrogenetic modelling of in situ fractional crystallization in the zoned Loch Doon pluton, Scotland. *Contributions to Mineralogy and Petrology* **78**, 196-207.

Toselli, A. J., Rossi de Toselli, J. N. & Rapela, C. W. (1978). El basamento metamorfico de la Sierra de Quilmes, Republica Argentina. *Revista de la Asociacion Geologica Argentina* **33**, 105-121.

van der Molen, I. & Paterson, M. S. (1979). Experimental deformation of partially-melted granite. *Contributions to Mineralogy and Petrology* **70**, 299-318.

Varela, R., Basei, M. A. S., González, P. D., Sato, A. M., Naipauer, M., Neto, M. C., Cingolani, C. A. & Meira, V. T. (2011). Accretion of Grenvillian terranes to the southwestern border of the Río de la Plata craton, western Argentina. *International Journal of Earth Sciences* **100**, 243-272.

Vernon, R. H., Etheridge, M. A. & Wall, V. J. (1988). Shape and microstructure of microgranitoid enclaves: Indicators of magma mingling and flow. *Lithos* **22**, 1-11.

Vielzeuf, D. & Montel, J. M. (1994). Partial melting of metagreywackes. Part I. Fluid-absent experiments and phase relationships. *Contributions to Mineralogy and Petrology* **117**, 375-393.

Watson, E. B. (1996). Dissolution, growth and survival of zircons during crustal fusion: Kinetic principles, geological models and implications for isotopic inheritance. *Transactions of the Royal Society of Edinburgh, Earth Sciences* **87**, 43-56.

Watson, E. B. & Harrison, T. M. (1983). Zircon saturation revisited: temperature and composition effects in a variety of crustal magma types. *Earth and Planetary Science Letters* **64**, 295-304.

Watson, E. B., Vicenzi, E. P. & Rapp, R. P. (1989). Inclusion/host relations involving accessory minerals in high-grade metamorphic and anatectic rocks. *Contributions to Mineralogy and Petrology* **101**, 220-231.

Watt, G. R., Burns, I. M. & Graham, G. A. (1996). Chemical characteristics of migmatites: Accessory phase distribution and evidence for fast melt segregation rates. *Contributions to Mineralogy and Petrology* **125**, 100-111.

Watt, G. R. & Harley, S. L. (1993). Accessory phase controls on the geochemistry of crustal melts and restites produced during water-undersaturated partial melting. *Contributions to Mineralogy and Petrology* **114**, 550-566.

White, A. J. R. & Chappell, B. W. (1977). Ultrametamorphism and granitoid genesis. *Tectonophysics* **43**, 7-22.

White, R. W. & Powell, R. (2002). Melt loss and the preservation of granulite facies mineral assemblages. *Journal of Metamorphic Geology* **20**, 621-632.

Whitney, D. L. & Evans, B. W. (2010). Abbreviations for names of rock-forming minerals. *American Mineralogist* **95**, 185-187.

Wolf, M. B. & London, D. (1995). Incongruent dissolution of REE- and Sr-rich apatite in peraluminous granitic liquids: differential apatite, monazite, and xenotime solubilities during anatexis. *American Mineralogist* **80**, 765-775.

Yakymchuk, C. & Brown, M. (2014). Behaviour of zircon and monazite during crustal melting. *Journal of the Geological Society* **171**, 465-479.

Zimmermann, U. (2005). Provenance studies of very low- to low-grade metasedimentary rocks of the Puncoviscana complex, northwest Argentina. *Geological Society Special Publication* **246**, 381-416.

**FIGURE CAPTIONS**

Fig. 1. Map of the Sierras Pampeanas, NW Argentina, showing the location of the study area (Fig. 2) in the back-arc of the Famatinian Orogen. Modified after Hongn *et al*. (2010), Dahquist *et al*. (2016) and Rapela *et al*. (2016). WSP = Western Sierras Pampeanas, ESP = Eastern Sierras Pampeanas. Main ranges: Ac = Sierra de Aconquija, Am = Sierra de Ambato, An = Sierra de Ancasti, Ca = Sierra de Cachi, CUL = Sierra de Los Llanos–Ulapes, Fa = Sierra de Famatina, Fi = Sierra de Fiambala, PP = Sierra de Pie de Palo, SC = Sierras de Córdoba, SM = Sierra de Molinos, SNC = Sierra Norte de Córdoba, SQ = Sierra de Quilmes, SSL = Sierra de San Luis, VF = Sierra de Valle Fértil, Ve = Sierra de Velasco.

Fig. 2. Map of the Tolombón and Ovejeria complexes in the northern Sierra de Quilmes. The El Pichao shear zone thrusts the high-grade Tolombón and Ovejeria complexes in the north over cooler rocks of the Agua del Sapo complex in the south. Metamorphic grade increases from ~NE to SW in the Tolombón complex, with repetition of the metamorphic zones west of the Tolombón thrust. Another shear zone separates the Tolombón and Ovejeria complexes. Small circles mark representative locations where one or more samples were collected. Modified after Finch *et al*. (2017).

Fig. 3. Metatexite migmatites of the Sierra de Quilmes. (a) Patch-nebulitic metatexite (left-hand side) after a metapsammitic protolith from the Opx-metatexite zone, Tolombón complex, with leucosomes containing peritectic garnet and orthopyroxene. Leucosomes link into a one-metre zone of garnet-bearing leucogranite (right-hand side). Coin on left for scale. (b) and (c) Net-structured metatexite from the Grt-metatexite zone, Ovejeria complex. (b) Leucosomes oriented parallel and oblique to the sub-horizontal foliation, collecting in possible dilatant sites such as extensional shear planes (arrows) along with peritectic garnet (~20 mm). (c) Collapse structure in a lineation parallel leucosome, at a potential dilatant site containing peritectic garnet (~20 mm), indicating melt extraction. (d) Stromatic metatexite with residuum-poor leucosomes feeding into central pool of homogeneous leucogranitic magma. Grt-metatexite zone, Tolombón complex (from Finch *et al*., 2017). (e) Residual stromatic metatexite with peritectic garnet in leucosome. Thin, remnant leucosomes are interpreted as evidence for melt loss. Grt-metatexite zone, Tolombón complex. (f) Photomicrograph of garnet in leucosome of a stromatic metatexite.

Garnet is intergrown with rounded quartz and contains minor small, rounded biotite inclusions (inset), indicating a peritectic origin. Importantly, garnet shows no retrogression to biotite at its margins, indicating melt extraction (e.g. White & Powell, 2002). Opx-metatexite zone, Tolombón complex. Plane-polarised light.

Fig. 4. Diatexite migmatites of the Sierra de Quilmes. (a) Heterogeneous leucocratic diatexite from the Ovejeria complex containing peritectic garnet in leucosomes (~25 mm), and blocky-lenticular psammite schollen. Margins between leucocratic and residuum-rich zones are diffuse at the centimetre scale. (b) Residual diatexite from the Ovejeria complex. Peritectic cordierite (>80 vol.% of rock) forms a cumulate texture with interstitial Qtz+Pl (<10 vol.%) forming interconnected irregular veinlets, interpreted to mark melt extraction channels. (c) Schlieric granite containing peritectic garnet (arrow) and cordierite, and idiomorphic K-feldspar up to ~10 mm long. Note homogeneous appearance compared with diatexite in (a). (d) Diatexite from Tolombón complex showing separation of residuum-rich and melt-rich zones at the metre scale. Irregular leucocratic band in the top half of the image likely represents injected melt due to its discordant shape and lack of mafic selvedges. (e) Photomicrograph of a residual diatexite from Tolombón complex showing subhedral cordierite surrounded by a pool of quartz within a large, corroded K-feldspar grain. Quartz has cuspate terminations against rounded K-feldspar and biotite, interpreted to represent a component of crystallised melt. Cross-polarised light. (f) Leucocratic diatexite (left) grading into schlieric granite (right) by gradual decrease in ferromagnesian minerals and schlieren. Ovejeria complex. Photograph is ~2 m across.

Fig. 5. Felsic granitoids from the Tolombón (a–e) and Ovejeria complexes (f–g). (a) Tonalite with uniformly distributed biotite, containing small schollen with low aspect ratios. Crd-subsolidus zone, Tolombón complex. (b) Photomicrograph of tonalite in (a) showing the characteristic microstructure defined by a framework of zoned plagioclase crystals touching at grain edges and corners, rich in muscovite inclusions oriented along crystallographic planes, with interstitial Qtz+Pl±Kfs±Bt±Sil. Cross-polarised light. (c) Fine-grained leucogranite with small magmatic garnet (~3 mm; arrow), and Ms-Sil-Bt schlieren with leucocratic rim. Finely laminated biotite layers define a faint foliation. (d) Medium-grained (~5 mm) garnet-bearing pink granite intruding a stromatic metatexite lit-par-lit with straight margins. The host rock is the residual stromatic metatexite in Fig. 3e. (e) Pink granite, containing variably retrogressed cordierite, intruding lit-par-lit into a

stromatic metatexite. The margins of this intrusion are irregular with some seamless connection with leucosome in the metatexite. (f) Intrusion of coarse-grained (10–20 mm) pink granite with large garnet porphyroblasts (~30 mm) into a diatexite. Margins between host rock and granite intrusion are highly irregular. Small patches of pink granite and single K-feldspar grains are isolated from the intrusion (arrows), interpreted to represent disaggregation of pink granite within diatexite. (g) Nodule of Grt+Bt+Sil+Qtz within coarse-grained pink granite, indicating breakdown of garnet porphyroblasts.

Fig. 6. Backscattered electron (BSE) images showing the textures of the major accessory phases (zircon, monazite, and apatite) in the different rock types. (a) Prismatic (AR ~1:3) to elongate (AR ~1:5) zircon within Qtz in a Bt-rich domain of a diatexite. (b) Stubby (AR ~1:1, top-right corner) to prismatic (bottom-left corner) zircon grains proximal to a Bt-rich zone within schlieric granite. The different aspect ratios (AR) may reflect grain shapes or a cutting effect. (c) Blocky to hexagonal monazite along Qtz-Grt grain boundaries within a diatexite, proximal to stubby zircon grains. (d) Small monazite crystals (arrows) on the surface of corroded apatite in the leucosome of a metatexite. Dissolution of apatite in peraluminous melt can give rise to a boundary layer saturated in LREE causing monazite precipitation (Wolf & London, 1995).

Fig. 7. Bivariate major element plots for Sierra de Quilmes migmatites and granites of $SiO_2$ vs (a) ASI (mol. $Al_2O_3/(CaO + Na_2O + K_2O)$), (b) $FeO_T + MgO$, and (c) $K_2O$, and (d) $K_2O$ vs. $CaO + Na_2O$, all in wt %. Light grey field represents Puncoviscana Formation. Leucogranitic field based on data from NE Sierra de Quilmes (SQ) from Rapela (1976), Rapela & Shaw (1979), Becchio *et al*. (1999), Lucassen *et al*. (2001), and from Sierra de Molinos (SM) from Sola *et al*. (2013). Experimental melts from dehydration of muscovite-biotite schist (MBS) at 750° C, 6 kbar, and muscovite schist (MS) at 800° C, 6 kbar from Patiño Douce & Harris (1998). In (b) Sierra de Quilmes samples define two trends, one parallel to the Puncoviscana Formation (PV trend) comprising mostly leucocratic migmatites (grey squares and triangles) and schlieric granite (white symbols), and the other (SQ trend), a steeper one, linking the pure biotite end-member to felsic granitoids through a number of residual migmatites. Dashed arrow in (c) represents the steep positive trend in $K_2O$ *versus* $SiO_2$ from tonalites through leucogranites to pink granites.

Fig. 8. $FeO_T$ + MgO *vs* $K_2O$ (wt %) for Sierra de Quilmes migmatites and granites, divided into fields of residual and leucocratic migmatites, schlieric granites, tonalites leucogranites, and pink granites. Light grey field represents the Puncoviscana Formation (PV) protolith. Felsic granitoids define a sub-horizontal trend at the base of the plot that is also reflected by leucogranitic rocks in the literature (field with horizontal lines; Rapela, 1976; Rapela & Shaw, 1979; Becchio *et al*., 1999; Lucassen *et al*., 2001; Sola *et al*., 2013). MBS and MS from Patiño Douce & Harris (1998), see caption to Fig. 7 for details. Arrows represent vectors toward various mineral compositions.

Fig. 9. Bivariate trace element plots for Sierra de Quilmes migmatites and granites: $LREE_T$ (a), Th (b), Zr (c), and U (d) *vs* $FeO_T$ + MgO. For $FeO_T$ + MgO > 3.8 wt %, trace elements in migmatites and schlieric granites form a cloud lacking an obvious trend. For $FeO_T$ + MgO < 3.8 wt.%, trace elements of felsic granitoids are generally positively correlated, however U shows an ill-defined positive trend in (d). Leucogranitic rocks from the literature typically agree with the trends of the felsic granitoids, as indicated by the fields marked with horizontal stripes. Thick horizontal line is the average concentration of trace elements for samples with $FeO_T$ + MgO >3.8 wt %. Dashed horizontal line is the average upper continental crust (UCC) concentration (Rudnick & Gao, 2003), and dotted horizontal line the average Puncoviscana Formation (PV) concentration (Supplementary Data Electronic Appendix 4). Thick grey lines are saturation values of $LREE_T$ (a), estimated from Rapp & Watson (1986), and Zr (c), from Boehnke *et al*. (2013), assuming a peraluminous melt at ~800 °C with M=1.2, the average value of felsic granitoids.

Fig. 10. Chondrite-normalised (Sun & McDonough, 1989) REE abundances of: (a) residual migmatites, (b) leucocratic migmatites, (c) schlieric granites, (d) tonalites, (e) leucogranites, and (f) pink granites from the Sierra de Quilmes. Grey field represents the Puncoviscana Formation (PV) protolith. Wide variations in HREE patterns in (a) and (b) probably relate to the presence or absence of garnet in the sample.

Fig. 11. Simplified version of the $FeO_T$ + MgO *vs* $K_2O$ plot shown in Fig. 8. The thick shaded arrow indicates progressive filtering of residuum from the residual migmatites (dark grey, top end) to leucogranites (white, bottom end). Dotted arrows represent fractional crystallisation trends of leucogranitic magma towards early-crystallising Pl-rich tonalites (left-hand side), and evolved Kfs-rich fractionated pink granites (right-hand side).

Leucocratic migmatites and schlieric granites have analogous compositions to the Puncoviscana Formation, which we interpret to reflect mobilisation of residuum. MBS and MS from Patiño Douce & Harris (1998), see caption to Fig. 7 for details.

Fig. 12. Thorium (a) and Zr (b) *vs* U. Dashed line in (a) shows the weak positive trend ($R^2$: 0.46) between Th and U for felsic granitoids, compared to no trend observed between Zr and U in (b). Though Th and U are contained in both monazite and zircon, the stronger trend with Th is interpreted to indicate a greater control exerted by monazite. Grey field is the Puncoviscana Formation (PV) protolith.

Fig. 13. Multi-element plot normalised to the average upper continental crust (UCC; Rudnick & Gao, 2003), showing that leucogranites are mostly depleted in trace elements relative to the UCC, whereas the residual migmatites are enriched. Tonalites and pink granites (not shown) reveal similar patterns. Schlieric granites more closely approximate the composition of the UCC.

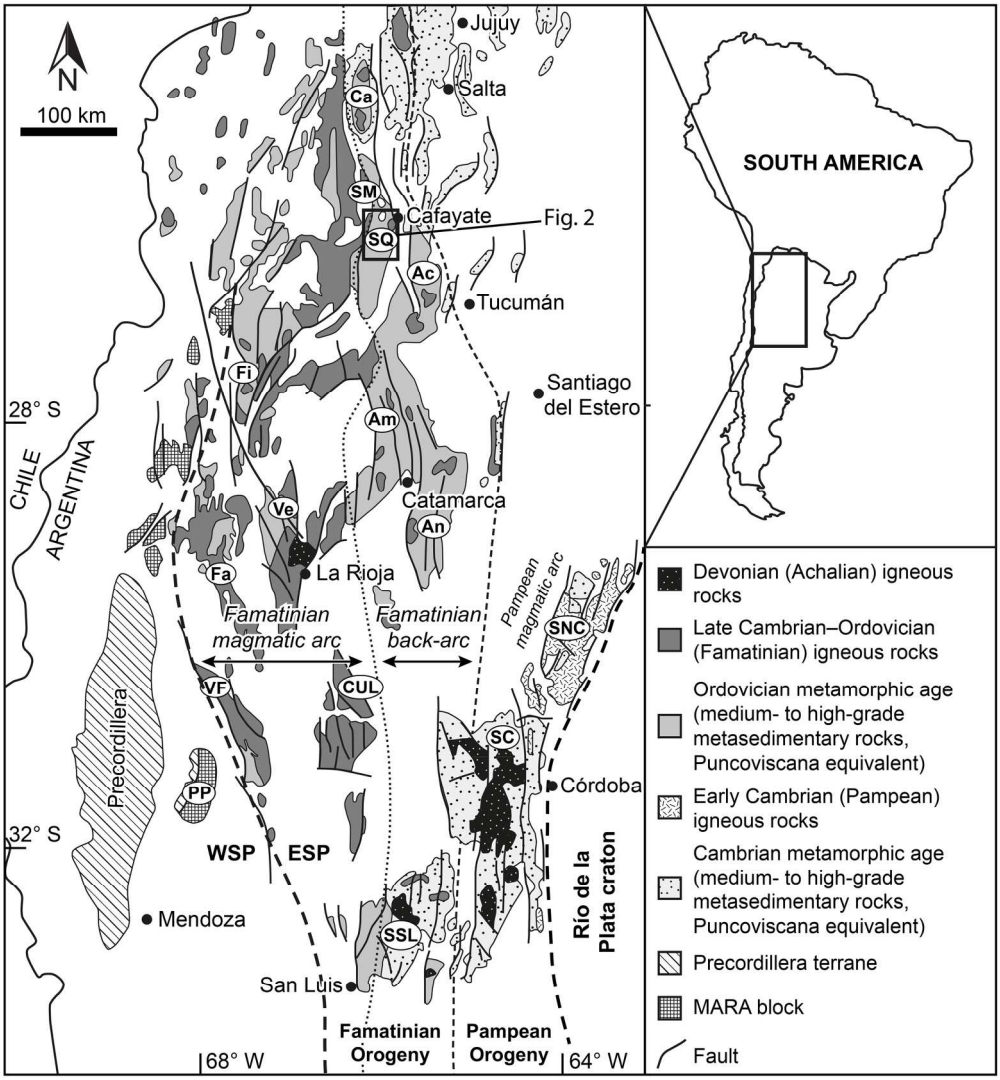


Figure 1

178x193mm (300 x 300 DPI)

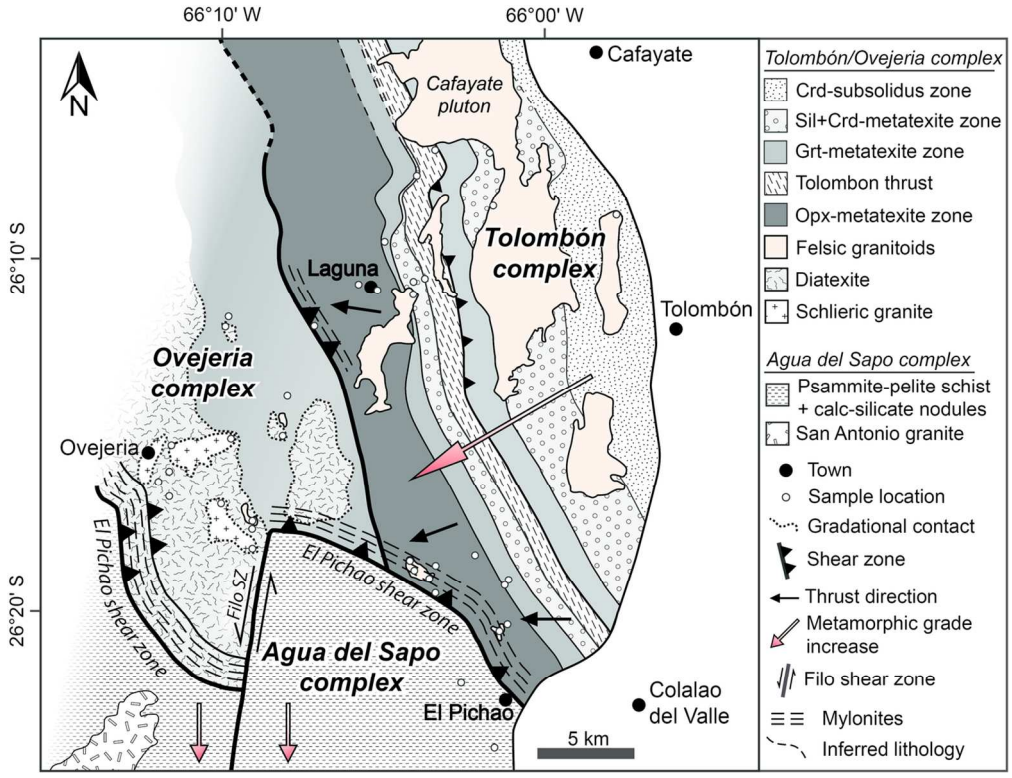


Figure 2

126x97mm (300 x 300 DPI)

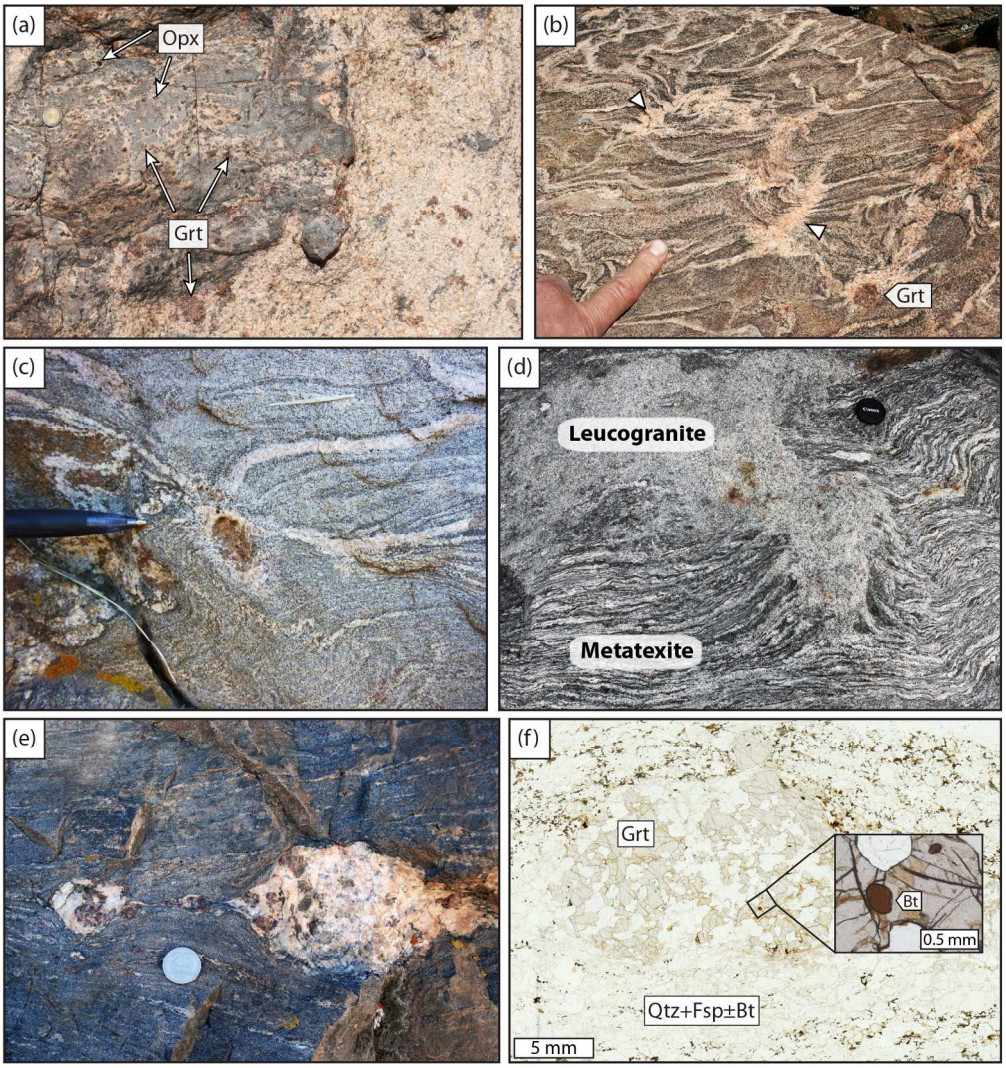


Figure 3

165x175mm (300 x 300 DPI)

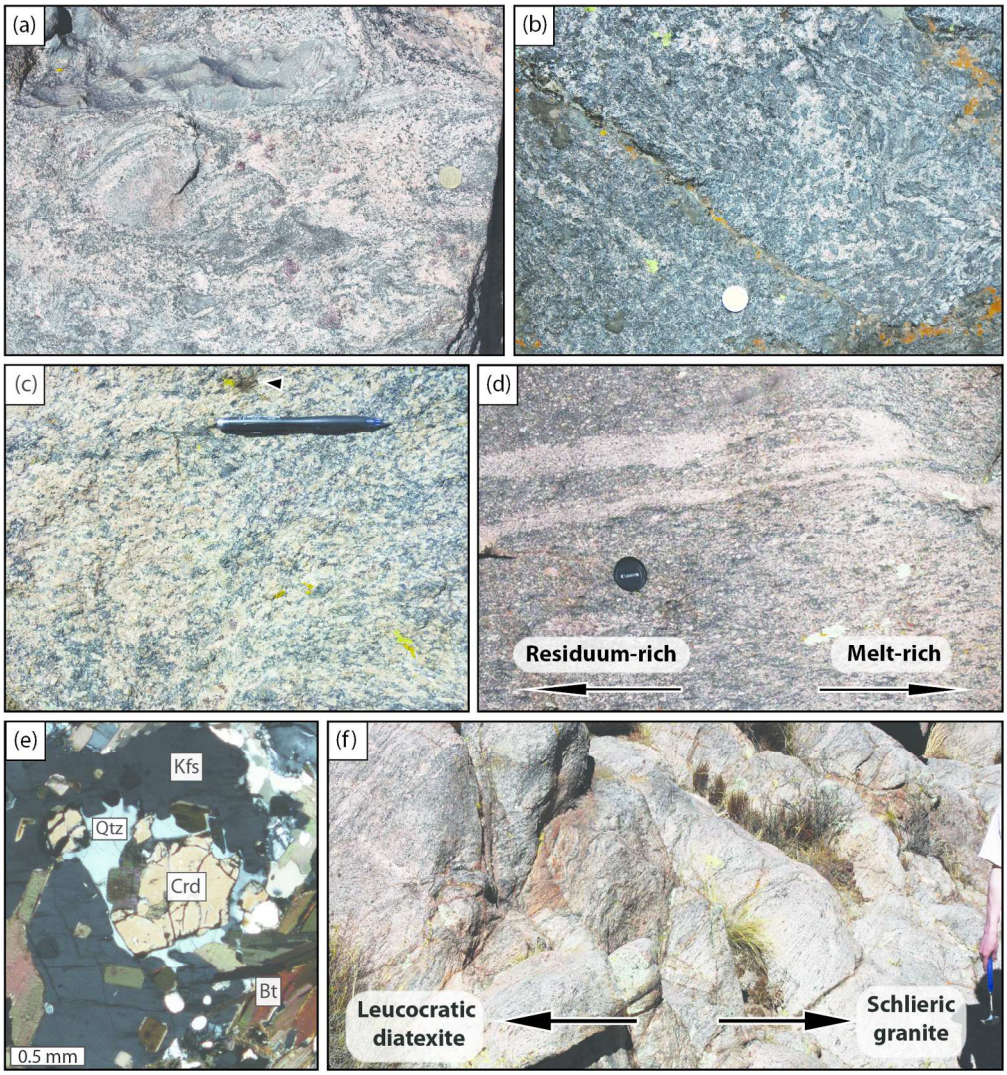


Figure 4

165x176mm (300 x 300 DPI)

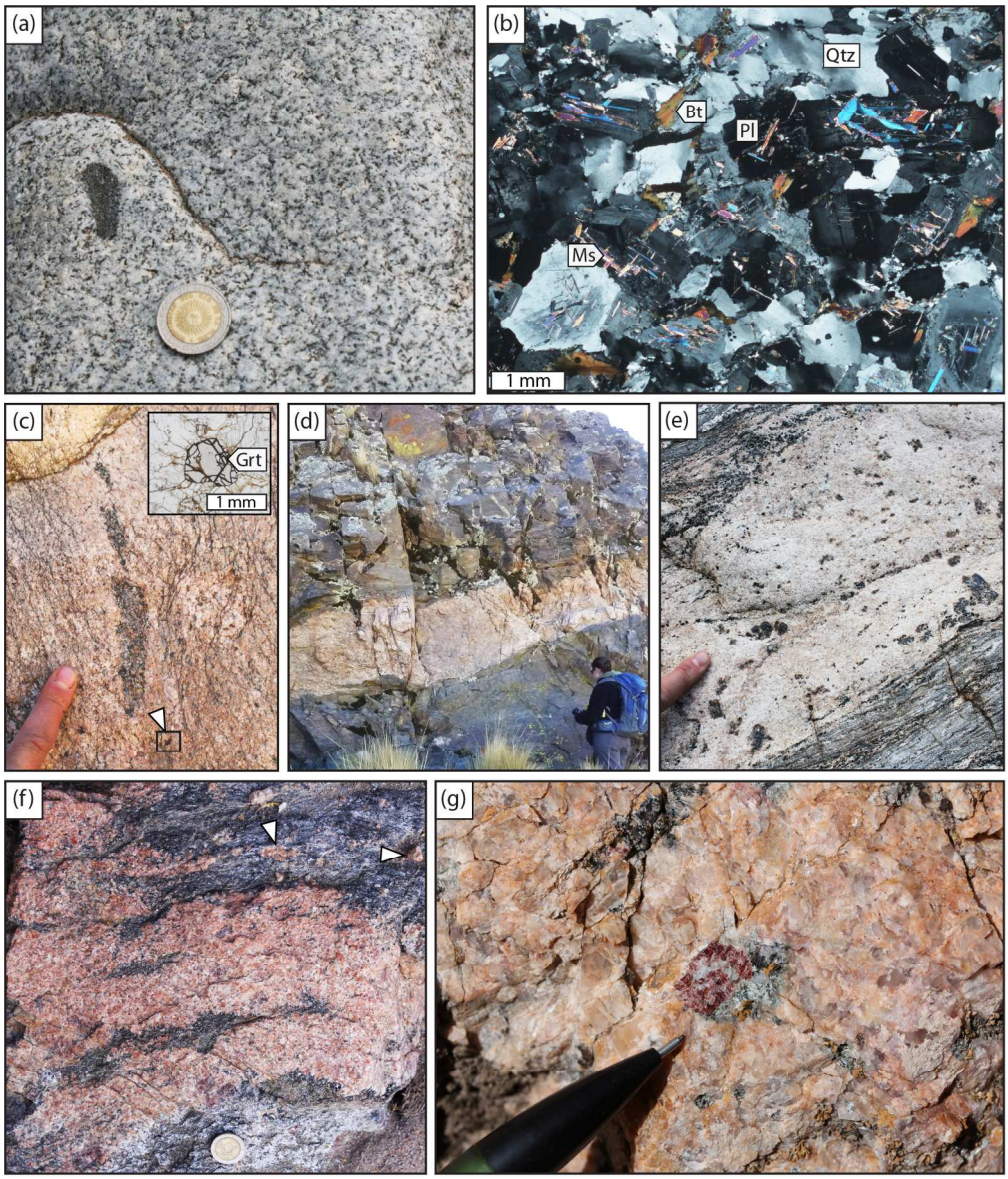


Figure 5

165x193mm (300 x 300 DPI)

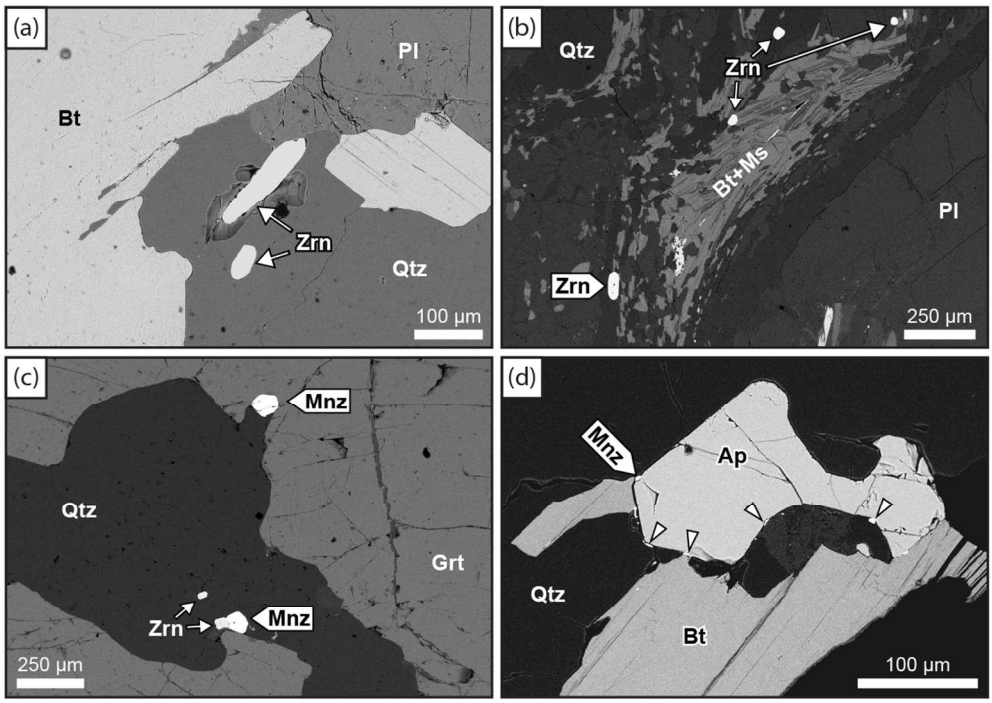


Figure 6

109x77mm (300 x 300 DPI)

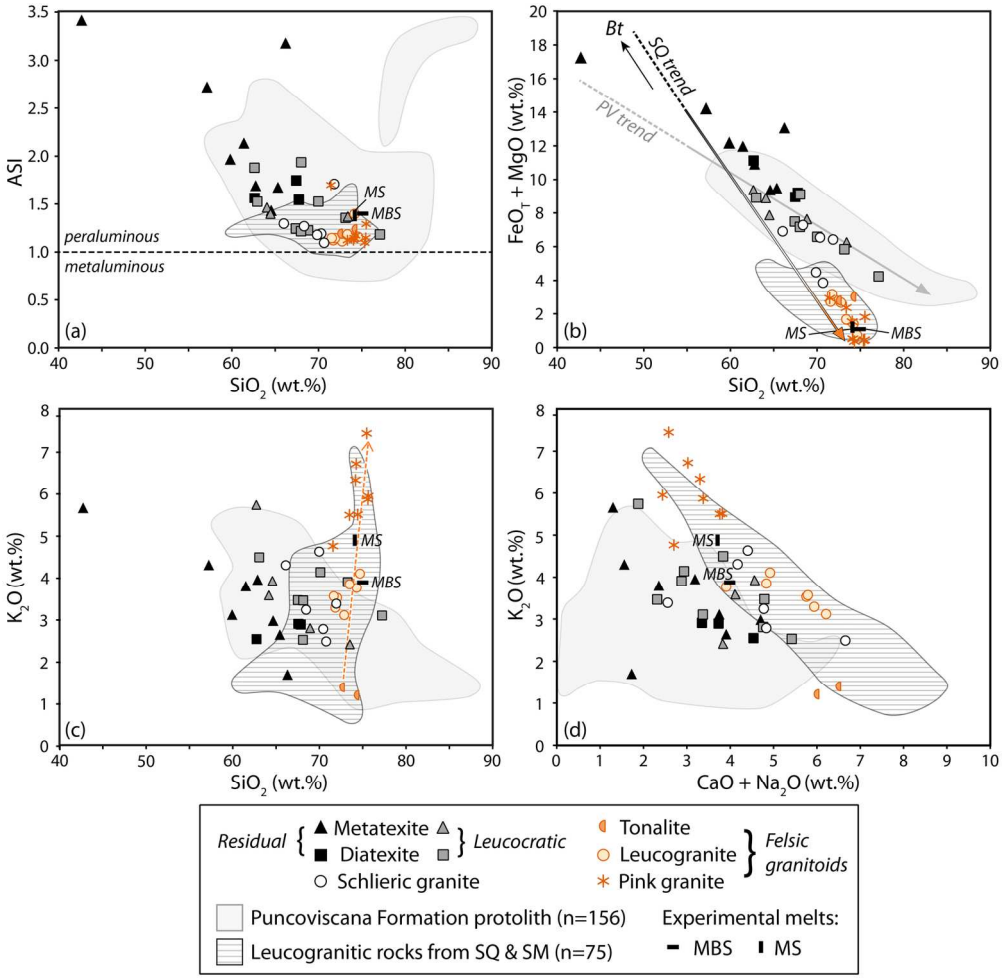


Figure 7

161x157mm (300 x 300 DPI)

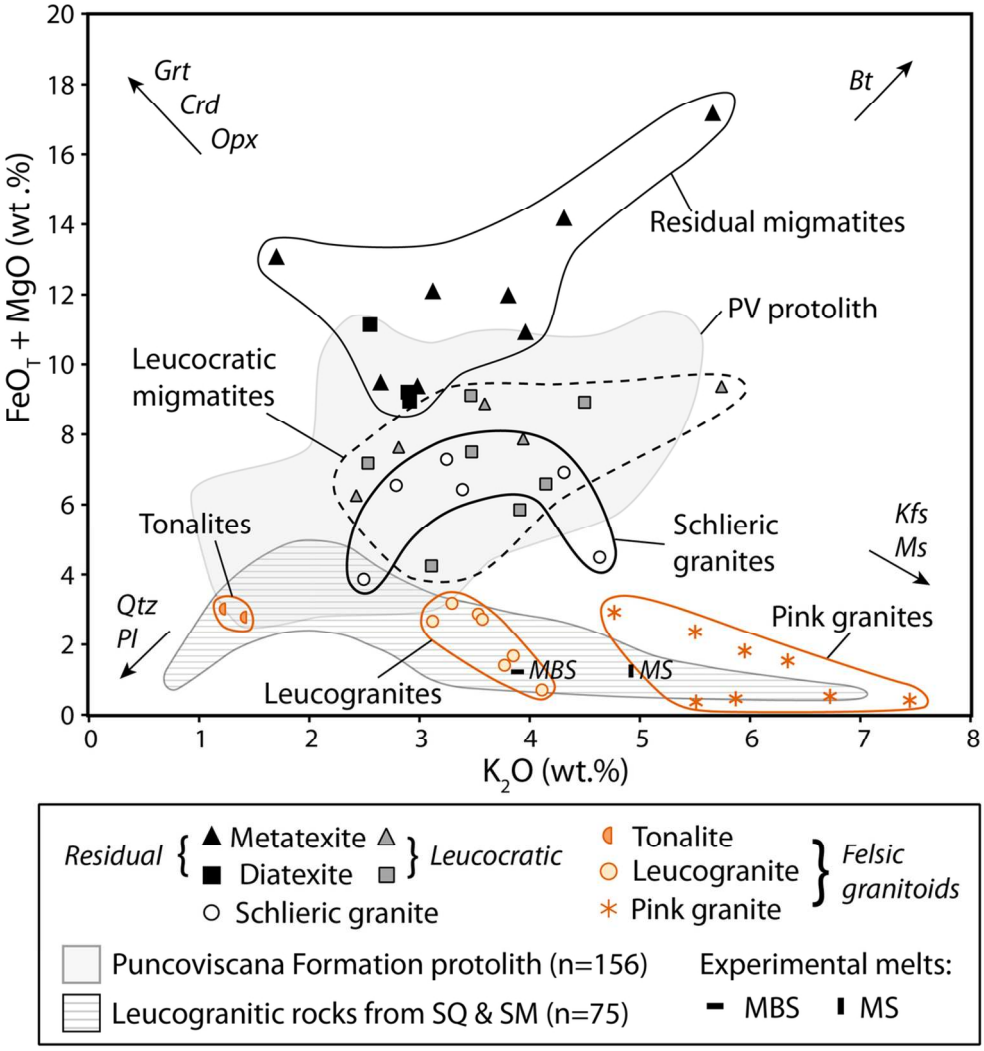


Figure 8

110x116mm (300 x 300 DPI)

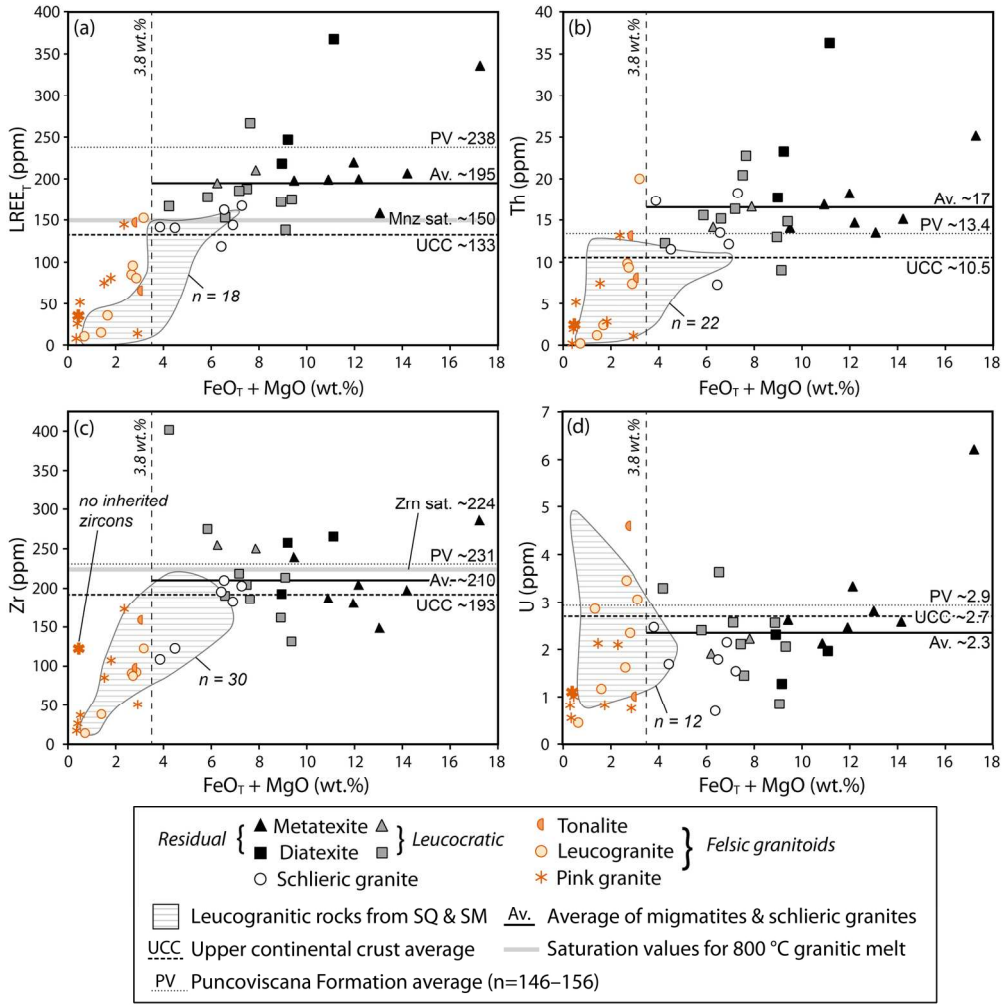


Figure 9

168x171mm (300 x 300 DPI)

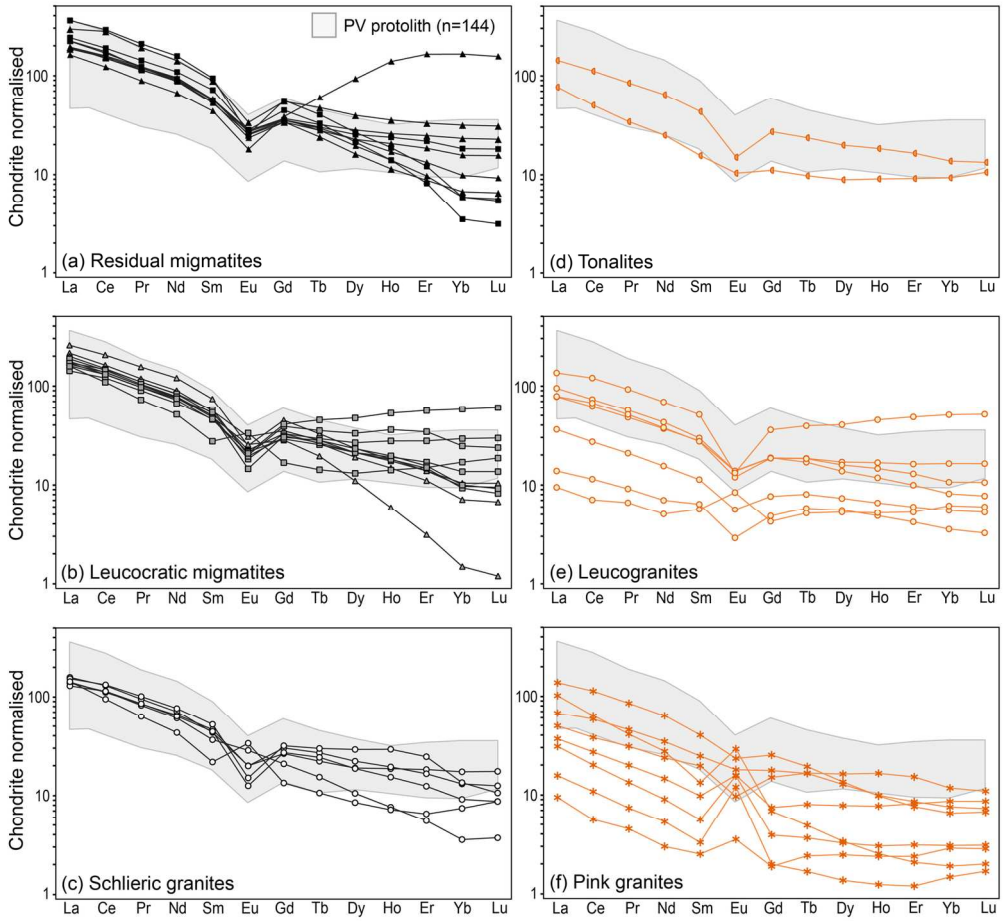


Figure 10

153x142mm (300 x 300 DPI)

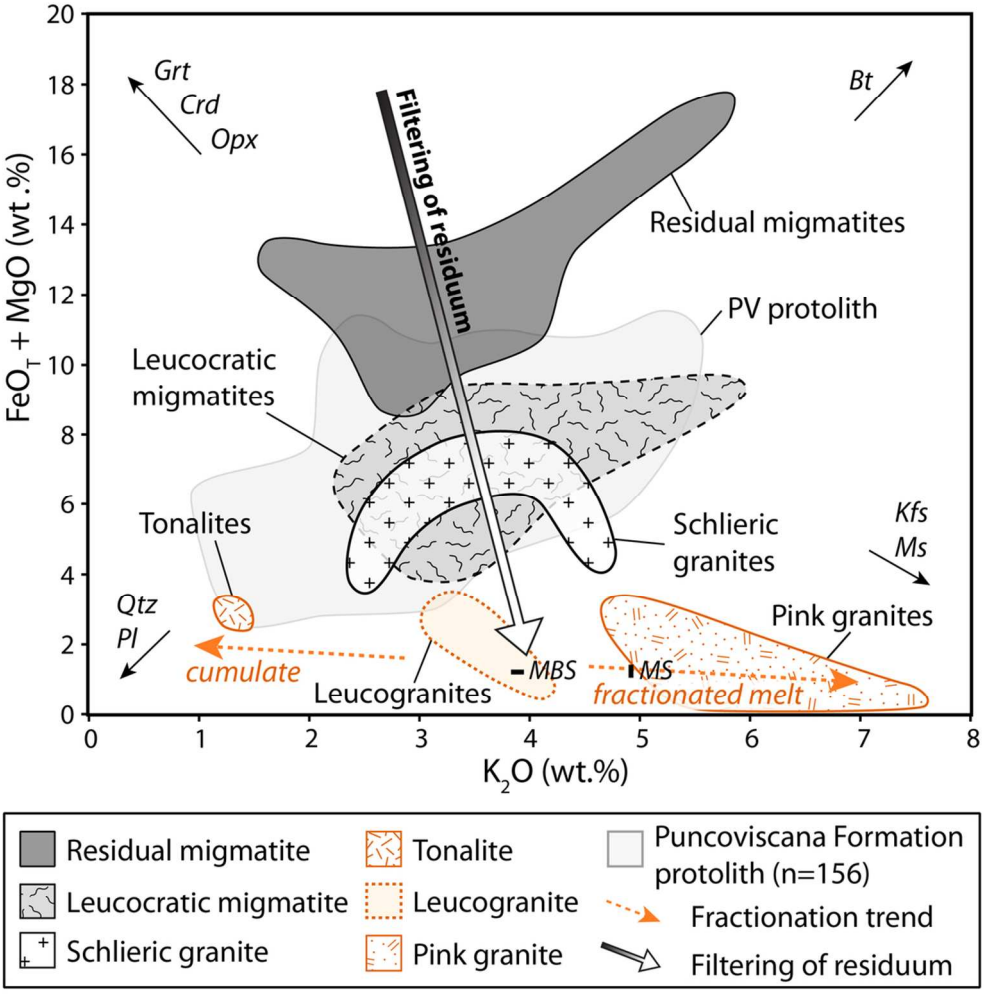


Figure 11

104x103mm (300 x 300 DPI)

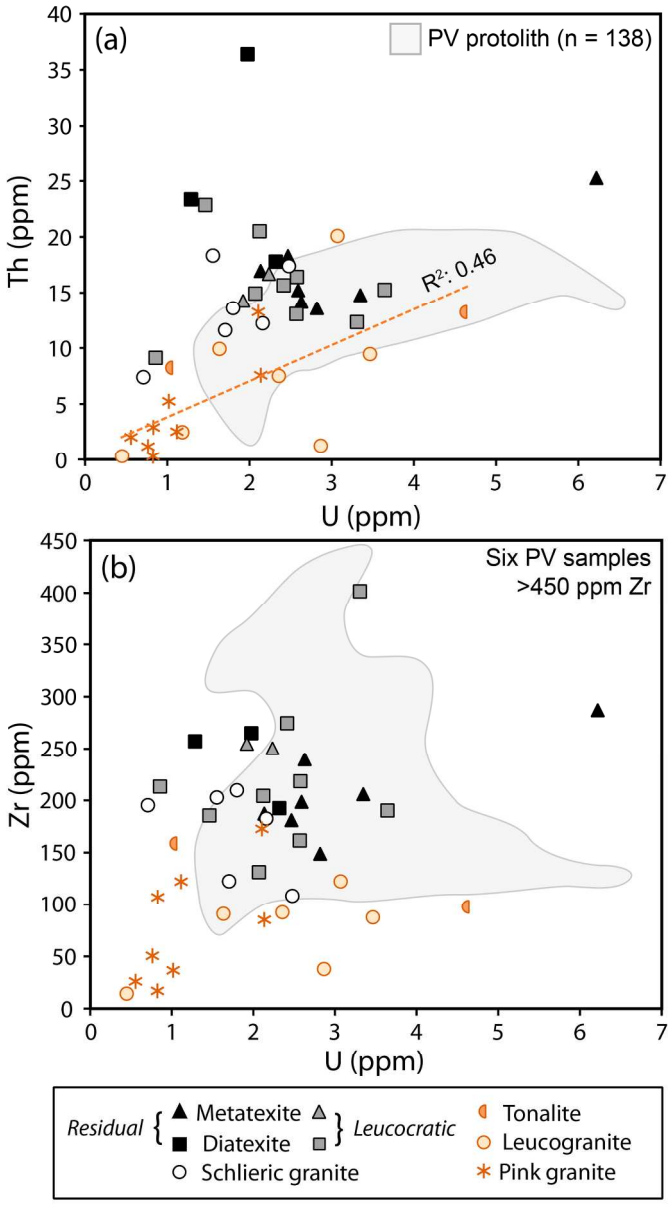


Figure 12

143x256mm (300 x 300 DPI)

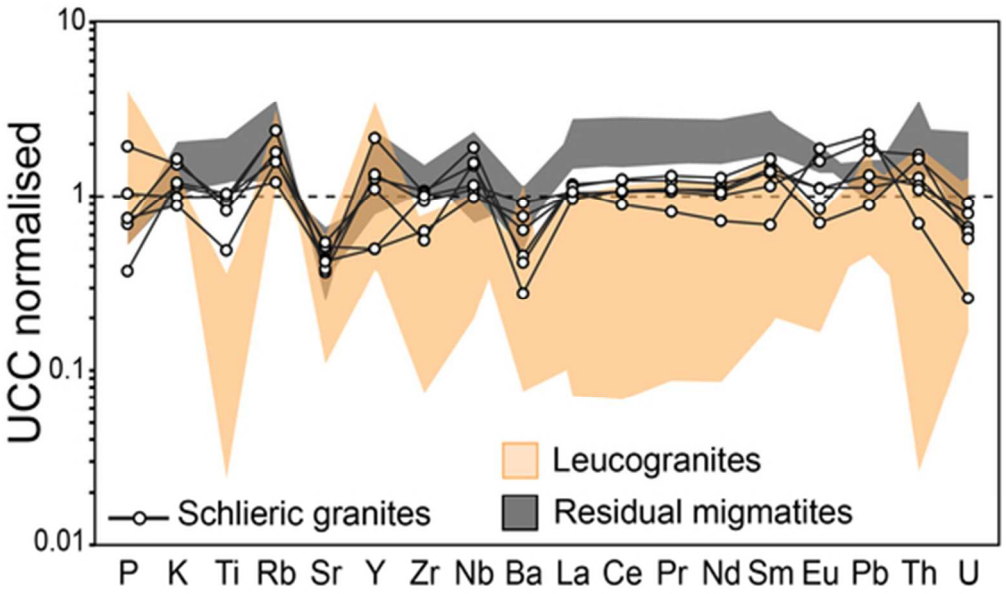


Figure 13

46x27mm (300 x 300 DPI)

**Table 1.** Whole-rock major and trace elements of Sierra de Quilmes rocks

| **Lithology** | **Psammite** | **Pelite** | | | | **Residual metatexite** | | | | **Leucocratic metatexite** | | **Leucocratic diatexite** | | | |
|---|---|---|---|---|---|---|---|---|---|---|---|---|---|---|---|
| Sample | Punco2b | Punco1 | Punco2a | SQ93 | SQ181b | SQ49 | SQ58A | SQ73A1 | SQ119B | SQ55 | SQ358 | SQ149 | SQ136V | SQ294C | SQ345 |
| *Major elements (wt.%)* | | | | | | | | | | | | | | | |
| | 70.39 | 73.23 | 61.51 | 63.25 | 68.40 | 59.82 | 57.14 | 64.54 | 66.20 | 64.05 | 62.61 | 77.07 | 68.00 | 69.97 | 67.38 |
| | 0.73 | 0.63 | 0.77 | 0.80 | 0.69 | 1.04 | 1.16 | 1.03 | 0.28 | 0.76 | 1.18 | 0.54 | 0.88 | 0.54 | 0.72 |
| $_3$ | 13.25 | 13.06 | 17.26 | 16.29 | 13.79 | 19.22 | 19.89 | 16.05 | 15.25 | 15.98 | 17.59 | 10.75 | 14.94 | 14.43 | 14.94 |
| $_3$ [a] | 4.58 | 3.40 | 7.00 | 6.28 | 5.12 | 8.43 | 9.45 | 6.48 | 10.33 | 6.11 | 6.20 | 3.12 | 6.27 | 4.77 | 5.30 |
| MnO | 0.08 | 0.01 | 0.13 | 0.15 | 0.12 | 0.15 | 0.09 | 0.10 | 0.55 | 0.08 | 0.02 | 0.04 | 0.11 | 0.07 | 0.10 |
| MgO | 2.09 | 1.38 | 3.11 | 2.56 | 2.12 | 3.74 | 4.75 | 2.88 | 2.72 | 2.77 | 3.17 | 1.12 | 2.84 | 1.81 | 2.20 |
| | 0.94 | 0.32 | 0.63 | 2.46 | 1.82 | 1.44 | 0.58 | 1.60 | 0.67 | 1.54 | 0.28 | 1.06 | 0.87 | 0.84 | 2.13 |
| O | 2.47 | 2.06 | 1.58 | 3.92 | 2.92 | 2.30 | 0.97 | 3.10 | 1.06 | 2.58 | 1.60 | 2.31 | 1.45 | 2.09 | 2.65 |
| | 2.64 | 3.36 | 4.38 | 2.44 | 2.58 | 3.12 | 4.31 | 2.98 | 1.70 | 3.59 | 5.74 | 3.11 | 3.46 | 4.14 | 3.47 |
| | 0.18 | 0.17 | 0.12 | 0.18 | 0.19 | 0.18 | 0.17 | 0.15 | 0.09 | 0.22 | 0.16 | 0.12 | 0.05 | 0.11 | 0.10 |
| LOI | 1.96 | 2.47 | 2.98 | 1.37 | 1.44 | 1.18 | 1.70 | 0.90 | 0.74 | 1.83 | 1.87 | 0.55 | 0.76 | 1.10 | 0.84 |
| Total | 99.31 | 100.10 | 99.49 | 98.33 | 97.75 | 100.70 | 100.20 | 99.80 | 99.59 | 99.50 | 100.42 | 99.78 | 99.63 | 99.89 | 99.82 |
| [b] | 1.54 | 1.72 | 2.03 | 1.20 | 1.26 | 1.97 | 2.72 | 1.43 | 3.18 | 1.46 | 1.88 | 1.18 | 1.94 | 1.53 | 1.24 |
| *Trace elements (ppm)* | | | | | | | | | | | | | | | |
| | 78.75 | 63.66 | 118.73 | | | 136.07 | 163.98 | | 60.70 | | 151.95 | 52.79 | 132.21 | 71.75 | 85.38 |
| | 81.08 | 54.15 | 119.00 | | | 146.43 | 167.62 | | 106.10 | | 112.84 | 44.03 | 85.73 | 71.67 | 72.36 |
| | 114.55 | 137.26 | 196.63 | | | 148.27 | 176.50 | | 57.12 | | 234.13 | 121.06 | 102.60 | 171.88 | 173.69 |
| | 102.09 | 61.92 | 94.82 | | | 109.02 | 103.50 | | 71.52 | | 118.03 | 139.53 | 138.91 | 129.92 | 116.79 |
| | 34.56 | 30.32 | 29.61 | | | 35.97 | 16.21 | | 221.19 | | 8.37 | 29.12 | 21.33 | 31.05 | 56.71 |
| | 149.57 | 152.43 | 140.49 | | | 205.93 | 198.56 | | 148.87 | | 131.30 | 401.46 | 213.24 | 190.28 | 204.31 |
| | 12.39 | 12.17 | 17.21 | | | 17.42 | 18.78 | | 3.35 | | 22.34 | 11.56 | 16.90 | 10.76 | 23.37 |
| | 6.93 | 11.98 | 10.38 | | | 7.06 | 7.35 | | 4.48 | | 6.78 | 3.75 | 4.05 | 4.20 | 4.38 |
| | 357.39 | 295.41 | 425.11 | | | 402.31 | 711.16 | | 277.64 | | 740.81 | 486.58 | 576.59 | 414.53 | 249.48 |
| | 4.32 | 4.49 | 4.03 | | | 5.66 | 5.47 | | 1.28 | | 0.83 | 4.33 | 2.04 | 2.25 | 1.58 |
| | 0.95 | 0.98 | 1.25 | | | 1.20 | 1.26 | | 0.55 | | 1.53 | 1.02 | 1.35 | 1.06 | 1.53 |
| | 19.04 | 8.02 | 17.36 | | | 16.63 | 20.41 | | 14.22 | | 29.37 | 22.28 | 35.75 | 24.58 | 20.58 |
| | 11.06 | 11.75 | 16.02 | | | 14.77 | 15.21 | | 13.57 | | 14.92 | 12.32 | 9.11 | 15.25 | 20.50 |
| | 2.54 | 2.19 | 2.44 | | | 3.35 | 2.59 | | 2.82 | | 2.07 | 3.31 | 0.86 | 3.64 | 2.12 |
| | 36.85 | 29.66 | 45.16 | | | 43.87 | 45.72 | | 38.12 | | 38.96 | 37.63 | 37.23 | 33.49 | 40.35 |
| | 73.45 | 65.80 | 92.46 | | | 93.38 | 96.31 | | 74.32 | | 83.83 | 79.46 | 66.43 | 73.26 | 89.49 |
| | 8.88 | 7.23 | 9.81 | | | 11.27 | 11.62 | | 8.37 | | 9.56 | 9.15 | 6.83 | 8.49 | 10.39 |
| | 34.30 | 27.38 | 35.60 | | | 42.55 | 44.32 | | 30.82 | | 35.21 | 33.46 | 23.74 | 31.05 | 38.83 |
| | 7.60 | 6.12 | 7.20 | | | 8.60 | 8.74 | | 6.62 | | 7.28 | 6.88 | 4.16 | 6.96 | 8.71 |
| | 1.41 | 1.10 | 1.26 | | | 1.59 | 1.44 | | 1.03 | | 1.46 | 1.23 | 1.91 | 1.11 | 1.14 |
| | 6.64 | 5.59 | 6.04 | | | 7.45 | 6.88 | | 7.82 | | 5.73 | 5.88 | 3.41 | 6.12 | 7.90 |
| | 1.08 | 0.90 | 0.94 | | | 1.18 | 0.88 | | 2.23 | | 0.72 | 0.94 | 0.53 | 1.04 | 1.30 |
| | 6.24 | 5.37 | 5.40 | | | 7.07 | 4.06 | | 23.44 | | 2.76 | 5.31 | 3.29 | 5.82 | 8.32 |
| | 1.32 | 1.15 | 1.14 | | | 1.45 | 0.64 | | 7.83 | | 0.33 | 1.07 | 0.79 | 1.10 | 2.02 |
| | 3.52 | 3.16 | 3.07 | | | 4.04 | 1.43 | | 27.09 | | 0.51 | 2.78 | 2.45 | 2.55 | 5.63 |
| | 0.48 | 0.44 | 0.43 | | | 0.61 | 0.19 | | 4.21 | | 0.05 | 0.37 | 0.39 | 0.30 | 0.71 |
| | 3.13 | 2.88 | 2.87 | | | 3.90 | 1.13 | | 27.92 | | 0.25 | 2.29 | 2.86 | 1.68 | 4.15 |
| | 0.46 | 0.43 | 0.44 | | | 0.57 | 0.16 | | 3.95 | | 0.03 | 0.34 | 0.47 | 0.23 | 0.60 |
| $LREE_T$ | 161.07 | 136.19 | 190.23 | | | 199.67 | 206.71 | | 158.25 | | 174.84 | 166.57 | 138.39 | 153.24 | 187.76 |

$_2O_3$ taken as total FeO; [b]ASI: mol. $Al_2O_3/(CaO + Na_2O + K_2O)$; BD: below detection

**Table 1.** (continued)

| **Lithology** | **Schlieric granite** | | | | | **Tonalite** | **Leucogranite** | | | | | **Pink granite** | | | | |
|---|---|---|---|---|---|---|---|---|---|---|---|---|---|---|---|---|
| Sample | SQ136W | SQ291A | SQ292 | SQ301B | SQ337A | SQ86 | SQ74 | SQ75 | SQ337B | SQ337C | SQ372A | SQ38B | SQ130B | SQ539 | SQ545D | SQ548 |
| *Major elements (wt.%)* | | | | | | | | | | | | | | | | |
| | 71.81 | 70.30 | 69.84 | 68.33 | 70.64 | 74.14 | 74.16 | 73.33 | 72.71 | 71.70 | 74.54 | 75.49 | 74.27 | 75.31 | 74.02 | 75.45 |
| | 0.67 | 0.64 | 0.53 | 0.64 | 0.32 | 0.31 | 0.13 | 0.19 | 0.20 | 0.16 | 0.02 | 0.43 | 0.03 | 0.03 | 0.11 | 0.04 |
| $^{3}$ | 13.77 | 13.53 | 14.76 | 14.78 | 15.39 | 14.43 | 14.85 | 14.52 | 14.70 | 14.63 | 14.66 | 13.75 | 14.49 | 13.57 | 13.95 | 13.77 |
| $^{3}$ [a] | 4.35 | 4.59 | 3.22 | 5.39 | 2.76 | 2.26 | 1.08 | 1.46 | 1.92 | 2.49 | 0.59 | 1.07 | 0.29 | 0.30 | 1.19 | 0.33 |
| MnO | 0.08 | 0.07 | 0.03 | 0.16 | 0.04 | 0.06 | 0.11 | 0.03 | 0.03 | 0.17 | 0.06 | 0.01 | 0.01 | BD | BD | BD |
| MgO | 2.08 | 1.95 | 1.27 | 1.90 | 1.10 | 0.76 | 0.32 | 0.21 | 0.75 | 0.69 | 0.11 | 0.74 | 0.07 | 0.11 | 0.34 | 0.12 |
| | 0.98 | 2.23 | 1.54 | 1.63 | 2.23 | 2.88 | 0.70 | 0.80 | 1.73 | 1.39 | 0.87 | 1.15 | 0.71 | 0.41 | 0.72 | 0.53 |
| O | 1.58 | 2.61 | 2.87 | 3.15 | 4.42 | 3.11 | 3.21 | 4.04 | 4.08 | 4.23 | 4.03 | 1.29 | 3.11 | 2.17 | 2.58 | 2.84 |
| | 3.39 | 2.79 | 4.63 | 3.24 | 2.49 | 1.21 | 3.77 | 3.85 | 3.12 | 3.29 | 4.11 | 5.95 | 5.51 | 7.45 | 6.34 | 5.87 |
| | 0.06 | 0.16 | 0.11 | 0.10 | 0.11 | 0.06 | 0.61 | 0.49 | 0.08 | 0.11 | 0.11 | 0.08 | 0.15 | 0.16 | 0.23 | 0.21 |
| | 0.77 | 0.86 | 0.82 | 0.94 | 0.75 | 1.02 | 1.23 | 1.26 | 0.87 | 1.10 | 0.69 | 0.76 | 0.82 | 0.49 | 0.59 | 0.66 |
| Total | 99.52 | 99.73 | 99.62 | 100.26 | 100.26 | 100.23 | 100.17 | 100.17 | 100.18 | 99.95 | 99.80 | 100.73 | 99.45 | 100.00 | 100.08 | 99.82 |
| [b] | 1.71 | 1.19 | 1.18 | 1.27 | 1.10 | 1.24 | 1.40 | 1.18 | 1.11 | 1.12 | 1.16 | 1.29 | 1.17 | 1.10 | 1.12 | 1.15 |
| *Trace elements (ppm)* | | | | | | | | | | | | | | | | |
| | 86.45 | 75.23 | 64.19 | 69.70 | 31.22 | 21.51 | 5.73 | 21.48 | 19.18 | 20.47 | 1.33 | 20.50 | 4.14 | 3.12 | 10.40 | 4.09 |
| | 105.93 | 67.97 | 54.74 | 85.90 | 45.98 | 47.16 | 81.26 | 13.72 | 34.17 | 28.25 | 16.24 | 12.73 | 5.28 | 3.13 | 22.91 | 3.20 |
| | 102.12 | 137.43 | 152.18 | 202.34 | 133.62 | 35.69 | 264.12 | 242.28 | 122.58 | 122.77 | 93.53 | 148.10 | 135.82 | 166.05 | 160.61 | 150.21 |
| | 136.53 | 140.98 | 165.89 | 123.93 | 175.29 | 181.10 | 35.01 | 67.77 | 168.58 | 181.29 | 125.79 | 197.30 | 42.39 | 210.03 | 161.73 | 141.01 |
| | 10.59 | 26.89 | 10.56 | 45.80 | 23.31 | 14.84 | 7.97 | 12.53 | 23.78 | 72.83 | 8.63 | 3.73 | 4.06 | 5.38 | 17.62 | 14.02 |
| | 195.38 | 209.71 | 122.57 | 202.74 | 108.53 | 158.78 | 37.88 | | 90.87 | 122.47 | 14.33 | 107.14 | 16.98 | 26.10 | 85.08 | 122.17 |
| | 14.04 | 18.20 | 11.89 | 23.07 | 18.86 | 4.29 | 7.82 | 12.34 | 12.19 | 8.71 | 2.38 | 8.60 | 0.65 | 1.29 | 4.68 | 2.81 |
| | 2.81 | 5.20 | 5.10 | 4.23 | 3.14 | 3.00 | 39.76 | 14.63 | 2.05 | 1.71 | 1.17 | 2.79 | 1.15 | 1.45 | 3.76 | 9.33 |
| | 577.52 | 289.12 | 483.17 | 264.35 | 176.40 | 175.31 | 47.55 | 121.04 | 298.51 | 312.14 | 721.20 | 980.04 | 77.37 | 873.18 | 327.90 | 554.02 |
| | 1.84 | 2.14 | 2.22 | 0.62 | 2.47 | 3.99 | 1.11 | 1.57 | 2.69 | 3.34 | 0.71 | 3.11 | 0.81 | 0.88 | 1.32 | 2.62 |
| | 1.01 | 1.37 | 0.92 | 1.42 | 1.40 | 0.55 | 1.41 | 2.60 | 0.85 | 0.71 | 0.18 | 0.83 | 0.25 | 0.20 | 0.50 | 0.42 |
| | 38.80 | 19.30 | 35.69 | 31.37 | 15.26 | 8.47 | 12.43 | 7.85 | 17.45 | 19.25 | 33.43 | 50.37 | 31.43 | 30.32 | 44.22 | 41.86 |
| | 7.37 | 13.58 | 11.59 | 18.33 | 17.38 | 8.22 | 1.24 | 2.45 | 9.91 | 20.08 | 0.28 | 2.88 | 0.25 | 2.00 | 7.55 | 2.50 |
| | 0.71 | 1.80 | 1.70 | 1.55 | 2.48 | 1.02 | 2.87 | 1.18 | 1.63 | 3.07 | 0.45 | 0.83 | 0.83 | 0.56 | 2.14 | 1.12 |
| | 33.23 | 36.71 | 32.09 | 35.52 | 30.01 | 18.26 | 3.23 | 8.46 | 18.39 | 31.67 | 2.21 | 23.99 | 2.22 | 7.25 | 15.84 | 8.67 |
| | 56.76 | 78.13 | 68.07 | 79.58 | 68.44 | 30.66 | 6.90 | 16.41 | 40.70 | 72.70 | 4.27 | 38.49 | 3.40 | 12.17 | 35.42 | 16.44 |
| | 5.82 | 8.83 | 7.62 | 9.39 | 7.93 | 3.25 | 0.86 | 1.96 | 4.79 | 8.67 | 0.62 | 3.87 | 0.42 | 1.26 | 4.29 | 1.87 |
| | 19.59 | 32.19 | 27.49 | 34.84 | 28.69 | 11.65 | 3.23 | 7.13 | 17.31 | 31.84 | 2.32 | 12.74 | 1.38 | 4.18 | 16.03 | 6.75 |
| | 3.24 | 6.43 | 5.44 | 7.77 | 6.58 | 2.38 | 0.96 | 1.71 | 4.13 | 7.70 | 0.85 | 2.01 | 0.38 | 0.85 | 3.74 | 1.48 |
| | 1.90 | 1.13 | 1.61 | 0.85 | 0.71 | 0.60 | 0.17 | 0.32 | 0.68 | 0.76 | 0.48 | 1.67 | 0.20 | 0.90 | 1.03 | 0.91 |
| | 2.68 | 5.28 | 4.17 | 6.34 | 5.41 | 2.28 | 0.98 | 1.55 | 3.76 | 7.26 | 0.86 | 1.40 | 0.38 | 0.80 | 3.60 | 1.52 |
| | 0.39 | 0.81 | 0.56 | 1.09 | 0.88 | 0.36 | 0.21 | 0.30 | 0.68 | 1.45 | 0.19 | 0.18 | 0.09 | 0.14 | 0.61 | 0.30 |
| | 2.10 | 4.67 | 2.60 | 7.19 | 4.62 | 2.26 | 1.39 | 1.83 | 3.98 | 10.12 | 1.32 | 0.85 | 0.62 | 0.82 | 3.22 | 1.97 |
| | 0.40 | 1.03 | 0.42 | 1.61 | 0.85 | 0.51 | 0.27 | 0.37 | 0.82 | 2.52 | 0.29 | 0.14 | 0.13 | 0.17 | 0.56 | 0.43 |
| | 1.05 | 2.95 | 0.89 | 3.96 | 2.00 | 1.51 | 0.68 | 0.98 | 2.11 | 7.88 | 0.86 | 0.34 | 0.39 | 0.51 | 1.41 | 1.34 |
| | 0.16 | 0.43 | 0.10 | 0.44 | 0.25 | 0.23 | 0.09 | 0.14 | 0.28 | 1.23 | 0.14 | 0.05 | 0.06 | 0.08 | 0.20 | 0.21 |
| | 1.23 | 2.87 | 0.59 | 2.23 | 1.51 | 1.59 | 0.59 | 0.92 | 1.79 | 8.51 | 1.03 | 0.32 | 0.48 | 0.52 | 1.27 | 1.46 |
| | 0.22 | 0.43 | 0.09 | 0.26 | 0.22 | 0.27 | 0.08 | 0.13 | 0.27 | 1.29 | 0.15 | 0.05 | 0.07 | 0.08 | 0.18 | 0.22 |
| $LREE_T$ | 118.65 | 162.29 | 140.71 | 167.10 | 141.65 | 66.20 | 15.17 | 35.66 | 85.32 | 152.59 | 10.27 | 81.10 | 7.81 | 25.71 | 75.33 | 35.22 |

$Fe_2O_3$ taken as total FeO; [b]ASI: mol. $Al_2O_3/(CaO + Na_2O + K_2O)$; BD: below detection